

# From Specificity to Generality: Revisiting Generalizable Artifacts in Detecting Face Deepfakes

Long Ma<sup>1</sup>   Zhiyuan Yan<sup>2</sup>   Yize Chen<sup>3</sup>   Jin Xu<sup>4</sup>  
 Qinglang Guo<sup>1</sup>   Hu Huang<sup>1</sup>   Yong Liao<sup>1†</sup>   Hui Lin<sup>5</sup>

<sup>1</sup> School of Cyber Science and Technology, University of Science and Technology of China

<sup>2</sup> School of Electronic and Computer Engineering, Peking University

<sup>3</sup> School of Data Science, The Chinese University of Hong Kong

<sup>4</sup> School of Information Science and Technology, University of Science and Technology of China

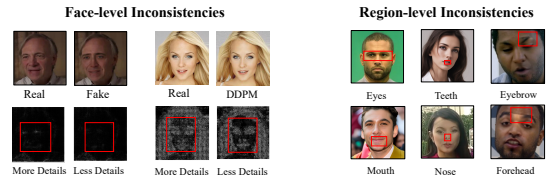
<sup>5</sup> China Academy of Electronics and Information Technology

{longm@mail, yliao@}ustc.edu.cn

## Abstract

Detecting deepfakes has been an increasingly important topic, especially given the rapid development of AI generation techniques. In this paper, we ask: How can we build a universal detection framework that is effective for most facial deepfakes? One significant challenge is the wide variety of deepfake generators available, resulting in varying forgery artifacts (e.g., lighting inconsistency, color mismatch, etc). But should we “teach” the detector to learn all these artifacts separately? It is impossible and impractical to elaborate on them all. So the core idea is to pinpoint the more common and general artifacts across different deepfakes. Accordingly, we categorize deepfake artifacts into two distinct yet complementary types: Face Inconsistency Artifacts (FIA) and Up-Sampling Artifacts (USA). FIA arise from the challenge of generating all intricate details, inevitably causing inconsistencies between the complex facial features and relatively uniform surrounding areas. USA, on the other hand, are the inevitable traces left by the generator’s decoder during the up-sampling process. This categorization stems from the observation that all existing deepfakes typically exhibit one or both of these artifacts. To achieve this, we propose a new data-level pseudo-fake creation framework that constructs fake samples with only the FIA and USA, without introducing extra less-general artifacts. Specifically, we employ a super-resolution to simulate the USA, while design a Blender module that uses image-level self-blending on diverse facial regions to create the FIA. We surprisingly found that, with this intuitive design, a standard image classifier trained only with our pseudo-fake

(a). Face Inconsistency Artifacts (FIA)



**Hint-1:** AI-generated faces often exhibit inconsistencies at both the face level and region level compared to the surrounding areas.

(b). Up-Sampling Artifacts (USA)



**Hint-2:** AI-generated faces often exhibit up-sampling artifacts by the decoders during the generation process.

Figure 1. Illustration of the two identified general forgery artifacts across different face deepfakes: (a) Face Inconsistency Artifacts and (b) Up-Sampling Artifacts. We show that the existing face deepfakes typically exhibit both or one of these two artifacts.

data can non-trivially generalize well to unseen deepfakes.

## 1. Introduction

In recent years, A growing number of facial manipulation techniques have advanced due to the rapid development of generative models [39, 40, 62, 80], which facilitate the production of highly realistic and virtually undetectable alterations. As a result, the risks of personal privacy being violated and the spread of misinformation have increased significantly. Therefore, developing a universal deepfake detector that can be used to detect the existing diverse fake methods has become an urgent priority.

In this paper, we pose the question: *How can we build*

<sup>†</sup> Corresponding Author.

Methods	Alteration artifact		Introduced Artifacts		
	global	local	Face Inconsistency		Up-Sampling
			face-level	region-level	
Face Xray [44], PCL [93], OST [4]	✓		✓		
SLADD [3]	✓			✓	
SBI [67]	✓		✓		
SeeABLE [41]		✓		✓	
RBI [68]	✓		✓		
<b>Ours</b>	✓	✓	✓	✓	✓

Table 1. **Comparison of our framework and Sota methods using pseudo-deepfake synthesis.** Our method differs from previous methods in terms of the level at which alterations are applied (local vs global), the introduced artifacts, and the level at which facial inconsistencies are applied.

*a universal detection framework that is effective for most facial deepfakes?* A significant challenge lies in the wide range of deepfake generators, which lead to different types of forgery artifacts such as lighting inconsistency and color mismatch. Specifically, a large number of existing works are dedicated to creating detection algorithms that are carefully designed to identify counterfeit artifacts within specific handcrafted designs, including eye blinking [46], pupil morphology [26], and corneal specularities [33]. However, these methods are mainly effective for identifying particular forgery techniques. But should we train the detector to learn each of these artifacts separately? It is impossible and impractical to cover them all. So, *where should we start from?*

The core idea is to encourage the detection model to learn the more generalizable artifacts. As indicated in previous works [67, 75, 84], different fakes might share some common forgery patterns, and the unlimited deepfake artifacts could be generalized and summarized by the limited generalizable artifacts. Motivated by this, we conduct an in-depth preliminary exploration of the common patterns of existing deepfake artifacts. After our preliminary exploration, we identify two generalizable deepfake artifacts and categorize them into two distinct yet complementary categories: Face Inconsistency Artifacts (FIA) and Up-Sampling Artifacts (USA), as depicted in Figure 1. FIA represents an inherent limitation that deepfakes struggle to overcome, originating from the generator’s incapacity to precisely reproduce facial attributes and nuances, as well as the inescapable disparities between regions induced by amalgamation processes. In contrast to FIA, USA is not readily apparent to the unaided eye and arises from an up-sampling process that the generator’s decoder cannot adequately substitute. Considering the intrinsic necessity for decoding and up-sampling within the generator’s operations, every facial manipulation method invariably introduces Up-Sampling Artifacts (USA). Numerous prior investigations have substantiated this observation [22, 70]. To date, all existing deepfakes characteristically display one or

both of these artifact categories.

To enable the model to simultaneously capture FIA and USA, we propose a sophisticated data augmentation method: **FIA-USA**, which leverages super-resolution models [76] and autoencoders [61] to introduce Up-Sampling Artifacts (USA) by reconstructing the face, and employs a strategy of generating multiple masks to blend the reconstructed face with the original, thereby introducing Face Inconsistency Artifacts (FIA) by creating discrepancies at both the facial and regional levels. Augmented with the aforementioned dual artifacts, our method effectively conditions the model to generalize across unseen deepfakes. Furthermore, to maximize the efficacy of FIA-USA, we introduce two complementary techniques: **Automatic Forgery-aware Feature Selection (AFFS)**, which streamlines feature dimensionality and augments feature discernment through adaptive selection. **Region-aware Contrastive Regularization (RCR)**, by juxtaposing the features of the manipulated region against those of the authentic region, RCR enhances the model’s focus on the up-sampling traces within the manipulated areas and the inconsistencies between different regions.

Our method surpasses the most recent state-of-the-art data augmentation methods [43, 44, 67, 68, 79, 86] on traditional deepfake benchmarks, and we have realized substantial improvements in generation deepfake benchmarks when compared to the baseline method. In addition, we perform cross-manipulation and cross-dataset detection evaluation on unseen data to align with real-world detection scenarios. Our method has shown enhanced generalization and robustness in the context of cross dataset generalization.

## 2. Related Work

**Deepfake Generation Methods.** In the field of forgery detection, the broad definition of deepfake detection encompasses both forged face image / video detection and generated image / video detection. In this paper, deepfake detection specifically refers to the detection of fake faces. Based on the methods by which fake faces are generated,

we categorize deepfakes into two types: traditional deepfake, and the generative deepfake. Traditional deepfake methods typically involve face replacement [13, 18, 47] and face reenactment [72, 73]. Facial replacement typically involves identity exchange using autoencoder-based [13] or graph based exchange methods [18], while facial reenactment employs reconstruction techniques to exchange faces from the source video to the target video while maintaining consistency in the identity of the target person. Unlike traditional deepfakes that involve local tampering, generative deepfakes directly generate fake faces through generative models [37, 38, 59, 61]. As discussed in some works [86, 87], the detection methods using RGB data augmentation methods have poor performance in this type of forgery, as these generation methods do not involve mixing operations. More importantly, an increasing number of facial tampering methods [39, 40, 40, 80] are evolving based on generation models, which implies that the fake faces generated by these new tampering methods will contain both the artifacts introduced by the generative models and the blend boundaries brought by the blend operations. To date, Most of the work only focuses on one forgery method and is ineffective for other forgery methods.

**Classic Deepfake Detection.** Classic deepfake detection can be categorized into multiple aspects: On the one hand, deepfake image detection, which can also be applied to deepfake video detection by computing the average value of multiple frames. Typical methods encompass data augmentation [44, 67, 86, 93], frequency-domain analysis [24, 36, 53, 60], identity information [9, 17, 74], contrastive learning [23, 91], network structure improvement [17, 92], watermark [77, 89], robustness [42, 55], interpretability [16, 66] and so forth. On the other hand, deepfake video detection innovative video representation formats [83], video-level data augmentation [79], self-supervised learning [2, 29, 96], anomaly detection [19, 20], biological signal [8, 81], multi-modal based [58]. In addition to the above two aspects, the the remainder of the work involves forgery localization [27, 55], multi task learning [55, 90], real scenario [69], adversarial attack [48], and so on.

### 3. Method

In this section, we begin by outlining two distinct and prevalent types of forgery artifacts found in deepfakes: **Face Inconsistency Artifacts (FIA)** and **Up-Sampling Artifacts (USA)**. We then detail the construction of data augmentation techniques (**FIA-USA**) designed to enable the model to learn to detect these artifacts concurrently. Subsequently, we present the **Automatic Forgery-aware Feature Selection (AFFS)** and **Region-aware Contrastive Regularization (RCR)**.

#### 3.1. Face Inconsistency Artifacts (FIA)

As depicted in Figure 1, Face Inconsistency Artifacts (FIA) frequently occur in deepfakes due to the inherent difficulty in rendering intricate details, which often results in discrepancies between intricate facial features and the more uniform surrounding regions. In essence, until deepfake technology advances to the point where it can flawlessly replicate real faces, these artifacts are likely to persist. We will now explore the origins of Face Inconsistency Artifacts by categorizing deepfake techniques into two domains: *Full Face Synthesis* and *Face Swapping*. In the case of full face synthesis deepfakes, the presence of Face Inconsistency Artifacts is primarily contingent upon the capabilities of the generator, which, regardless of their magnitude, are invariably present. For face swapping, these artifacts arise from two primary sources: **1).** the efficacy of the generator. **2).** the blending seam created during the face swapping’s blending procedure. Furthermore, we can categorize face swapping into two main types based on the forged area: *macro-editing* and *micro-editing*. Macro-editing can be further classified into two subtypes: editing based on 4 facial keypoints and editing based on 81 keypoints, whereas micro-editing allows for precise adjustments to each facial feature. **In section B of the appendix, we provide a detailed description of the classification of forgery techniques and their differences.**

#### 3.2. Up-Sampling Artifacts (USA)

Conversely, the artifacts invariably present in the forged regions produced by the forgery generator are due to the upsampling process within the generator’s decoder, known as Up-Sampling Artifacts (USA). The extent of USA introduced can differ among various generators. To investigate more universal upsampling artifacts, we categorize forgery techniques into two types: One category generates images of forged regions that are as clear and free of blur as the original image (using Diffusion models [61] and GANs [38] as the main methods, and upsampling the latent code through autoencoder (AE) to generate images). And another type result in blurred tampered areas, requiring additional facial super-resolution models (SR) to process the blurred areas.

#### 3.3. FIA-USA

We propose a new data augmentation method to generate pseudo-fake training samples, aiming to introduce FIA and USA present in forged faces. The core idea is to introduce FIA and USA simultaneously by blending the real image  $I_R$  and the reconstructed image  $I_F$ , as follows:

$$I_{PF} = M \odot I_F + (1 - M) \odot I_R, \quad (1)$$

where  $\odot$  represents the element wise multiplication operator,  $M$  represents the mask of the manipulated area, which

---

**Algorithm 1** Pseudocode for FIA-USA

---

**Input:** Base image  $I$  of size  $(H, W, 3)$ , facial landmarks  $L$  of size  $(81, 2)$

**Output:** Image  $I$  with FIA and USA

```
1: def  $\mathcal{T}(I)$  : ▷ Source-Target Augmentation
2:    $I \leftarrow \text{ColorTransform}(I)$ 
3:    $I \leftarrow \text{FrequencyTransform}(I)$ 
4:   return  $I$ 
5: def  $\text{Recon}(I)$  : ▷ Reconstruct the source image
6:   if  $\text{Uniform}(\min = 0, \max = 1) \in [0, 0.3]$  :
7:      $I_s \leftarrow \text{AE}(I)$ 
8:   else if  $\text{Uniform}(\min = 0, \max = 1) \in (0.3, 0.5]$  :
9:      $I_s \leftarrow \text{SR}(I)$ 
10:  else
11:     $I_s \leftarrow I$ 
12:  return  $I$ 
13:  $I_s, I_t \leftarrow \text{Recon}(I), I$ 
14: if  $\text{Uniform}(\min = 0, \max = 1) < 0.5$  :
15:    $I_s, I_t \leftarrow \mathcal{T}(I_s), I_t$ 
16: else :
17:    $I_s, I_t \leftarrow I_s, \mathcal{T}(I_t)$ 
18:  $M \leftarrow \text{CombineFacialFeatures}(L)$  or  $\text{ConvexHull}(L)$ 
19:  $M \leftarrow \text{MaskAugmentation}(M)$ 
20:  $I_{PF} \leftarrow I_s \odot M + I_t \odot (1 - M)$ 
```

---

varies between 0 and 1. We considered two ways of generating masks to cover all possible occurrences of FIA: 1) Mask erosion on the convex hull of the facial 81 or 4 keypoints, aimed at simulating macro-editing; 2) Random combination of facial features, aimed at simulating micro-editing. Consequently, we address generic USA through three approaches: **1.** Employ an autoencoder (AE) to reconstruct the entire image [61]. **2.** Enhance the facial details using a super-resolution model [76] (SR). **3.** Do not reconstruct the original image. Formally speaking, we introduced different levels of FIA through blending operations and reconstructed images, while introducing USA for forged areas through reconstructed images. Please refer to Algorithm 1 for the complete algorithmic process. Table 1 compares the differences between our proposed FIA-USA method and the previous blend-based data augmentation method. **In section C of the appendix, we provide more information on blend-based data augmentation and FIA-USA.**

### 3.4. Loss Function

In addition to FIA-USA, which aims to generate fake training samples from real training samples, we also propose **Automatic Forgery aware Feature Selection (AFFS)** and **Region aware Contrastive Regularization (RCR)** based on FIA-USA.

#### 3.4.1. Automatic Forgery-aware Feature Selection

Before the model training begins, AFFS calculates the similarity between the feature map differences of each dimension of the real and fake faces in the each layer of the neural network and the mask  $M$ , sorts from high to low and selects the top  $m_i$  dimensions of features of the  $i$ -th layer to construct a Feature Pyramid Network (FPN) [49]. It is worth noting that AFFS is only performed before the model training starts, and once completed, which dimensions of each layer’s features will be used to construct the FPN is fixed. AFFS enables adaptive feature selection, reduces feature redundancy, enhances feature representativeness and discriminability, and ensures effective Region-aware Contrastive Regularization.

Specifically, given a neural network  $\phi$ , we define the output of  $i$ -th layer as  $f_i = \phi_i(I) \in \mathbb{R}^{W_i * H_i * C_i}$  where  $I \in \mathbb{R}^{H * W * 3}$  represents the input image,  $W_i$  and  $H_i$  refer to the size of the feature map, and  $C_i$  represents the feature dimension of  $i$ -th layer. Before training begins, we select the top  $m_i$  channels for the  $i$ -th layer by minimizing the following loss function.

$$\mathcal{L}_{AFFS}^{i,k} = \frac{1}{N} \sum_{n=1}^N \|\mathcal{F}(f_i^k(R_n) - (f_i^k(F_n)) - M_n)\|_2^2 \quad (2)$$

$\mathcal{F}$  represents normalization and scaling operations,  $f_i^k \in \mathbb{R}^{W_i * H_i}$ ,  $k \in [0, C_i]$ , represents the feature map of the  $k$ -th dimension of the  $f_i$ ,  $R_n$  and  $F_n$  are positive and negative samples generated by FIA-USA,  $M_n$  is the corresponding mask. Finally, we use the features  $f_i^k$  selected by AFFS to construct FPN, where  $f_i^k \in \mathbb{R}^{W_i * H_i * m_i}$ .

#### 3.4.2. Region-aware Contrastive Regularization

Given the network  $\phi$  and the Feature Pyramid Network (FPN)  $P$ , we first define a set of triplets  $F, R, M$ , where  $F$  and  $R \in \mathbb{R}^{H * W * 3}$  represents the pseudo-fake face and real face, and  $M \in \mathbb{R}^{H * W}$  represents the corresponding mask in FIA-USA used to generate the fake face. We denote the feature maps of real and fake faces as  $H_R = P(\phi(R))$ ,  $H_F = P(\phi(F))$ . For  $H_R$ , the areas inside and outside  $M$  are real, while for  $H_F$ , the areas inside  $M$  are manipulated and the areas outside  $M$  are real. We define the region within  $M$  as  $H_R^{in}$ ,  $H_F^{in}$  and the region outside  $M$  as  $H_R^{out}$ ,  $H_F^{out}$ . It is noteworthy that, aligning with LAA-Net [55], we acknowledge that pixels on the blend boundary are influenced by both false pixels within  $M$  and real pixels outside  $M$ , hence we discard pixel features on the blend boundary.

**Patch-level Contrastive Regularization.** For real faces, the features  $f$  of  $H_R^{in}$  and  $H_R^{out}$  are consistent, thus we aim to minimize the distance between them. Conversely, for fake faces, the features  $f$  of  $H_F^{in}$  and  $H_F^{out}$  are distinct, thus we aim to maximize the distance between them. Therefore, the loss function of **Patch-level Contrastive Regularization (PCR)** can be formulated as:

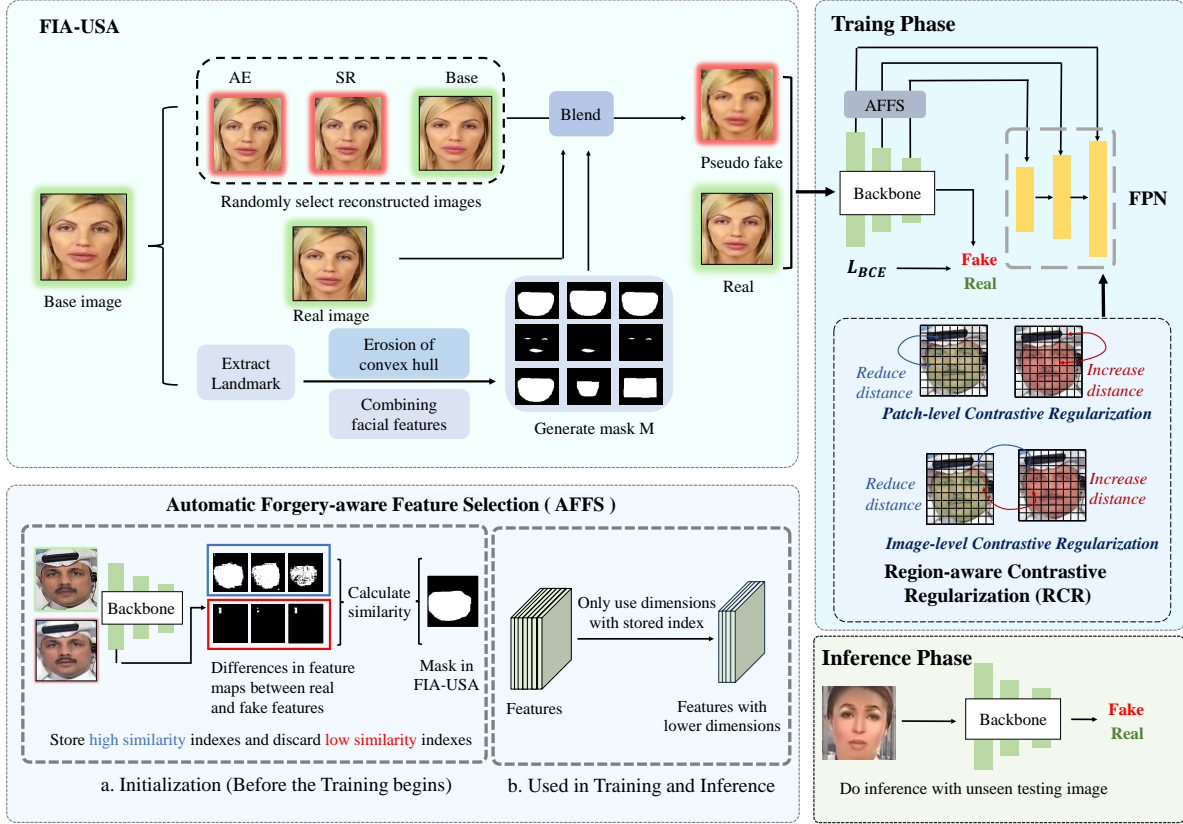


Figure 2. The overall framework of our proposed method consists of: 1) **FIA-USA**, which categorizes deepfake artifacts into Face Inconsistency Artifacts (FIA) and Up-Sampling Artifacts (USA). By employing data augmentation techniques, the model is enhanced to concurrently recognize and learn from both categories of artifacts. 2) **Region-aware Contrastive Regularization (RCR)**, which enables the model to focus simultaneously on forged boundaries and spatial artifacts through the contrastive regularization of features from forged and real regions. 3) **Automatic Forgery-aware Feature Selection (AFFS)**, which achieves efficient feature selection by assessing the similarity between the feature maps of each channel in each layer and the mask.

$$\mathcal{L}_1 = -\log \frac{\sum_{f_R \in H_R} e^{\delta(f_R^{in}, f_R^{out})/\tau}}{\sum_{f_R \in H_R} e^{\delta(f_R^{in}, f_R^{out})/\tau} + \sum_{f_F \in H_F} e^{\delta(f_F^{in}, f_F^{out})/\tau}}, \quad (3)$$

where  $\delta(\cdot)$  is the normalized cosine similarity between two features, as:

$$\delta(f_1, f_2) = \sum_{f_1^i \in f_1} \sum_{f_2^j \in f_2} \frac{f_1^i}{\|f_1^i\|} \cdot \frac{f_2^j}{\|f_2^j\|}, \quad (4)$$

where  $f^i$  represents a pixel feature.  $\tau$  is a temperature parameter.

**Image-level Contrastive Regularization.** Since both the region of real face and fake face outside  $M$  are real, we aim to minimize the distance between them and maximize the distance between the fake face and the real face in the area inside  $M$ . Therefore, the loss function for **Image-level**

**Contrastive Regularization (ICR)** can be formulated as:

$$\mathcal{L}_2 = -\log \frac{\sum_{f_{out} \in H^{out}} e^{\delta(f_R^{out}, f_F^{out})/\tau}}{\sum_{f_{out} \in H^{out}} e^{\delta(f_R^{out}, f_F^{out})/\tau} + \sum_{f_{in} \in H^{in}} e^{\delta(f_R^{in}, f_F^{in})/\tau}}. \quad (5)$$

**Overall Loss.** The network is optimized using the following loss:

$$\mathcal{L} = \lambda_1 \mathcal{L}_{BCE} + \lambda_2 \mathcal{L}_1 + \lambda_3 \mathcal{L}_2, \quad (6)$$

where  $\mathcal{L}_{BCE}$  denotes the cross-entropy classification loss.  $\mathcal{L}_{BCE}$ ,  $\mathcal{L}_1$  and  $\mathcal{L}_2$  are weighted by the hyperparameters  $\lambda_1$ ,  $\lambda_2$  and  $\lambda_3$ , respectively.

## 4. Experiments

### 4.1. Settings

**Datasets.** To evaluate the effectiveness of our proposed method, we conducted extensive experiments on multiple datasets, including both traditional and generative deepfake datasets.

**Traditional Deepfake Datasets.** FaceForensics++ (FF++) [63],

Detector	Backbone	Venues	CDF-v1	CDF-v2	DFD	DFDCP	Avg.
FWA [45]	Xception	CVPRW'18	0.790	0.668	0.740	0.638	0.714
CapsuleNet [56]	Capsule	ICASSP'19	0.791	0.747	0.684	0.657	0.720
CNN-Aug [30]	ResNet	CVPR'20	0.742	0.703	0.646	0.617	0.677
Face X-ray [44]	HRNet	CVPR'20	0.709	0.679	0.766	0.694	0.712
FFD [11]	Xception	CVPR'20	0.784	0.744	0.802	0.743	0.768
F3Net [60]	Xception	ECCV'20	0.777	0.798	0.702	0.735	0.749
SPSL [51]	Xception	CVPR'20	0.815	0.765	0.812	0.741	0.783
SRM [53]	Xception	CVPR'21	0.793	0.755	0.812	0.741	0.775
CORE [57]	Xception	CVPRW'22	0.780	0.743	0.802	0.734	0.764
Recce [2]	Designed	CVPR'22	0.768	0.732	0.812	0.734	0.761
SBI* [66]	EfficientNet-B4	CVPR'22	-	0.813	0.774	0.799	-
UCF [84]	Xception	ICCV'23	0.779	0.753	0.807	0.759	0.774
ED* [1]	ResNet-34	AAAI'24	0.818	<u>0.864</u>	-	<b>0.851</b>	-
ProDet† [6]	EfficientNet-B4	NeurIPS'24	<b>0.909</b>	0.842	<u>0.848</u>	0.774	0.843
LSDA* [86]	EfficientNet-B4	CVPR'24	0.867	0.830	<b>0.880</b>	0.815	<u>0.848</u>
Forensic-Adapter* [10]	CLIP (ViT-B/16)	CVPR'25	-	0.837	-	0.799	-
Ours	EfficientNet-B4	-	<u>0.901</u>	<b>0.867</b>	0.821	<u>0.818</u>	<b>0.852</b>

Table 2. **Cross-dataset Evaluations:** Cross-dataset evaluations were conducted using the **Frame-level AUC**. All experiments were trained on the c23 version of FF++ and tested on other datasets. ‘\*’ indicates the results are cited from [10] and ‘†’ indicates our reproduction results using the checkpoints provided by the authors, otherwise, the results are from DeepfakeBench [85].

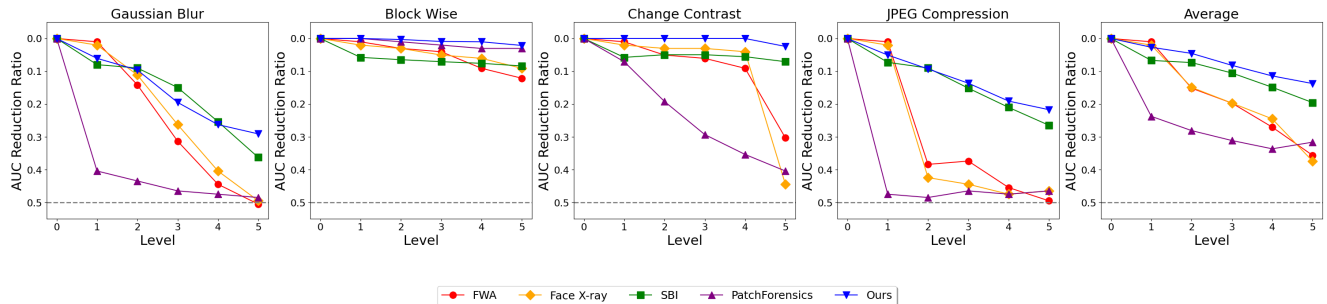


Figure 3. **Robustness to Unseen Perturbations.** We reported the Video-Level AUC Reduction Ratio for four specific types of perturbations at five different levels.

DeepfakeDetection (DFD) [12], Deepfake Detection Challenge (DFDC) [15], preview version of DFDC (DFDCP) [14], and CelebDF (CDF) [47]. FF++ comprises 1,000 original videos and 4,000 fake videos forged by four manipulation methods, namely, Deepfakes(DF) [13], Face2Face(F2F) [72], FaceSwap(FS) [18], and NeuralTextures(NT) [73]. Consistent with the SBI [67], we trained only with real faces from FF++. FF++ offers three levels of compression: raw, lightly compressed (c23), and heavily compressed (c40). Due to constraints regarding storage and download capabilities, we selected the c23 version of FF++, including DFD. Although many previous studies have utilized the same dataset for both training and testing, the preprocessing and experimental configurations can differ, making fair comparisons difficult. Therefore, in addition to testing on the raw data of the aforementioned datasets, we also performed generalization assessments on the unified new benchmark for traditional deepfakes, (DeepfakeBench) [85].

**Generative Deepfake Datasets.** Diffusion Facial Forgery (DiFF) [5] contains over 500,000 images synthesized using 13 different generation methods under four conditions: Text to Image (T2I), Image to Image (I2I), Face Swapping (FS) and Face Editing (FE). **Text to Image** encompasses four generation methods: *Midjourney* [54], *Stable Diffusion XL (SDXL)* [59], *Free-DoM-T* [88], and *HPS* [82]. **Image to Image** comprises *Low Rank Adaptation(LoRA)* [32], *DreamBooth* [64], *SDXL Refiner* [59], and *Free-DoM-I*. **Face Swapping** includes *DiffFace* [40] and *DC-Face* [40]. **Face Editing** comprises *Imagic* [39], *Cycle Diffusion(CycleDiff)* [80], and *Collaborative Diffusion(CoDiff)* [35]. Besides, we also conducted experiments on the latest deepfake dataset DF40 [87], which contains the forgery data generated within the FF++ domain, ensuring the evaluation fake methods different but the data domain unchanged.

**Evaluation Metrics.** We report the Frame-Level Area Under Curve (AUC) metric on the DeepfakeBench and DIFF dataset, re-

Method	Venues	uniface	e4s	facedancer	fsgan	inswap	simswap	Avg.
RECCE [2]	CVPR 2022	84.2	65.2	78.3	88.4	79.5	73.0	78.1
SBI [67]	CVPR 2022	64.4	69.0	44.7	87.9	63.3	56.8	64.4
CORE [57]	CVPRW 2022	81.7	63.4	71.7	<b>91.1</b>	79.4	69.3	76.1
IID [34]	CVPR 2023	79.5	71.0	79.0	86.4	74.4	64.0	75.7
UCF [84]	ICCV 2023	78.7	69.2	80.0	88.1	76.8	64.9	77.5
LSDA [86]	CVPR 2024	85.4	68.4	75.9	83.2	81.0	72.7	77.8
C DFA [50]	ECCV 2024	76.5	67.4	75.4	84.8	72.0	76.1	75.9
ProgressiveDet [6]	NeurIPS 2024	84.5	71.0	73.6	86.5	78.8	77.8	78.7
Ours	-	<b>91.8</b>	<b>87.5</b>	<b>83.0</b>	86.3	<b>87.4</b>	<b>91.0</b>	<b>87.8</b>

Table 3. We compared our method with state-of-the-art detection methods on six representative face swapping forgeries in DF40 [87].

Model	Venues	CDF-v2	DFDC	DFDCP
Face X-Ray [44]	CVPR’20	-	-	0.711
LipForensics [28]	CVPR’21	0.824	0.735	-
FTCN [94]	ICCV’21	0.869	-	0.740
PCL + I2G [93]	ICCV’21	0.900	0.675	0.743
HCIL [25]	ECCV’22	0.790	0.692	-
ICT [17]	CVPR’22	0.857	-	-
SBI [67]	CVPR’22	0.928	0.719	0.855
AltFreezing [79]	CVPR’23	0.895	-	-
SAM [7]	CVPR’24	0.890	-	-
LSDA [86]	CVPR’24	0.911	<b>0.770</b>	-
CFM [52]	TIFS’24	0.897	-	0.802
Ours	-	<b>0.941</b>	0.732	<b>0.866</b>

Table 4. **Comparison with SOTA methods using the Video-Level AUC.** The results of other methods are cited from their original papers.

port the Video-Level Area Under Curve (AUC) metric on the traditional deepfake datasets, to compare our proposed method with prior works.

**Implementation Details.** We utilize EfficientNetB4 [71] as the default neural network, and employ the SAM [21] optimizer to train it for 50 epochs. The batch size is set to 12. We uniformly sample 32 frames from each video during training. The initial learning rate is 0.001. For data augmentation, in addition to the proposed data augmentation (FIA-USA), RandomHorizontalFlip, RandomCutOut, and AddGaussian Noise were also applied. All experiments were conducted on a single NVIDIA 3090. We also investigate alternative network architectures and their respective outcomes. Empirically,  $\lambda_1, \lambda_2, \lambda_3$  are assigned values of 1, 2.5, 0.25. The temperature parameter  $\tau$  is 0.7. We also explored the impact of other variants on the detection results.

## 4.2. Generalization Evaluation

Our model’s generalization was evaluated on traditional and generation deepfake datasets at both the frame and video levels.

### 4.2.1. Traditional Deepfake Datasets

**Frame-level.** We first compare our method with previous work at the frame level. To ensure the fairness of the experiment, we conducted the experiment on the DeepfakeBench, and adhered

Method	Train Set		Test Subset			
	Real	Fake	T2I	I2I	FS	FE
Xception <sup>†</sup> [63]	✓	✓	62.43	56.83	85.97	58.64
F <sup>3</sup> -Net <sup>†</sup> [60]	✓	✓	66.87	67.64	81.01	60.60
EfficientNet <sup>†</sup> [71]	✓	✓	74.12	57.27	82.11	57.20
DIRE <sup>‡</sup> [78]	✓	✓	44.22	64.64	84.98	57.72
SBI <sup>†</sup> [67]	✓		80.20	80.40	85.08	68.79
Ours	✓		<b>86.05</b>	<b>84.95</b>	<b>89.42</b>	<b>72.73</b>

Table 5. **Comparison with universal deepfake detection methods using the Frame-Level AUC on the DiFF dataset.** ‘<sup>†</sup>’ indicates models that are designed for deepfake detection, while ‘<sup>‡</sup>’ signifies models intended for general generated image detection.

to the data preprocessing and experimental settings provided by them. For previous work, we utilized the experiment data provided by DeepfakeBench. As shown in Table 2, our method outperforms other methods on the majority of deepfake datasets and competes with state-of-the-art methods on the CDF-v1 dataset.

**Video-Level.** In addition to comparing at the Frame-Level, we also compared our method at the Video-Level with state-of-the-art detection algorithms, including various data augmentation methods. Typically, the experimental results are directly taken from the original paper and trained on the c23 version of FF++. FreqBlender [43] did not provide experimental results trained on the FF++ c23 version in their paper, therefore we directly cited experiment results on the FF++ raw version. The comparison results, as shown in Table 4, strongly demonstrate the effective generalization of our method, and our method outperforms other methods, even being comparable to FreqBlender trained on the raw version of FF++.

### 4.2.2. Generation Deepfake Datasets

As mentioned in Section 2, researchers have found that RGB enhancement methods exhibit limited efficacy when facing generative deepfakes. Here, we compared multiple universal deepfake detection methods on the generative deepfake dataset DiFF, as shown in Table 3 and Table 5. Our method not only exhibits robust generalization capabilities on traditional deepfakes, but also showcases superior performance in generative deepfake detection. Compared to the baseline method, our approach achieved a significant improvement of nearly 5%.

Setting		Test Dataset				Avg.
		Traditional		Generative		
		CDF-v2	DFDCP	FS	FE	
w FIA-USA	w/o Mtm	91.99	87.06	88.00	71.93	84.74
	w/o SR	93.25	86.81	80.73	61.07	80.46
	w/o AE	92.53	86.37	88.67	70.31	84.47
w RCR	w/o PCR	90.12	86.13	89.61	66.87	83.18
	w/o ICR	90.85	85.00	89.95	75.01	85.20
	w/o RCR	90.14	86.13	89.61	66.87	83.18
w/o FIA-USA		93.18	89.45	80.68	62.99	81.57
w/o AFFS		94.70	86.30	88.33	70.62	84.98
Ours		94.10	86.66	89.42	72.73	<b>85.72</b>

(a) **Ablation Study of Method Components.** We report the Video-Level AUC for traditional deepfake datasets and the Frame-Level AUC for generative deepfake datasets. Mtm denotes multiple types of masks, SR signifies the process of super-resolution, and AE refers to the reconstruction achieved through autoencoders.

Table 6. **Ablation experiment.** We conducted ablation experiments on method components, model frameworks, and hyperparameter configuration. The best results are presented in bold.

In section G of the appendix, we conducted experiments on more forgery techniques provided by DF40 and DIFF.

#### 4.2.3. Robustness

In Figure 3, we assessed the influence of different levels of random perturbations on the detection performance, the experimental setup adhering to the experimental protocols established in prior studies. We quantified the effects of different levels of Gaussian Blur, Block Wise, Change Contrast, Change Saturation, and JPEG Compression on the detectors. Notably, to gauge accuracy, we employed the reduction rate of Video-Level AUC to assess the robustness of the detector to different degrees of disturbance, which could be expressed as  $R_{AUC} = (AUC - AUC_{raw})/AUC_{raw}$ , where  $AUC_{raw}$  refers to no perturbations. Figure 3 shows that our method is more robust relative to other RGB-based methods. Change Contrast, Change Saturation, and JPEG Compression on the detectors. Notably, to gauge accuracy, we employed the reduction rate of Video-Level AUC to assess the robustness of the detector to different degrees of disturbance, which could be expressed as  $R_{AUC} = (AUC - AUC_{raw})/AUC_{raw}$ , where  $AUC_{raw}$  refers to no perturbations. Figure 3 shows that our method is more robust relative to other RGB-based methods.

#### 4.3. Ablation Study

**The impact of method components.** To evaluate the effectiveness of each component in our method, we performed ablation studies on multiple datasets. In Table 6a, we present the results of our ablation experiments on FIA-USA, Automatic Forgery-aware Feature Selection (AFFS), and Region-aware Contrastive Regularization (RCR), as well as the ablation of components in FIA-USA and RCR. The experimental results in the Table 6a underscore the efficacy of each component of our method. Notably, we report Video-Level AUC for traditional deepfake datasets and Frame-Level AUC for generative deepfake datasets.

**The impact of model framework.** Concurrently, we also examined the influence of various model architectures, as detailed in the Table 6b. We assessed the performance implications of EfficientNet [71], Resnet [30], and network layers on model performance. To ensure a fair comparison with ResNet, we extended training by

Model	Test Dataset						Avg.
	Traditional		Generative				
	CDF-v2	DFDCP	T2I	I2I	FS	FE	
Res50	82.45	79.14	74.73	76.94	68.82	58.59	73.44
Res101	85.51	82.35	73.21	74.95	71.26	60.44	74.62
Effb1	91.88	82.30	83.86	85.24	83.73	70.69	82.86
Effb4	94.10	86.66	86.05	84.95	89.42	72.73	<b>85.65</b>

(b) **Ablation Study on Model Architectures.**

$\lambda_1, \lambda_2, \lambda_3$	Test Dataset						Avg.
	Traditional		Generative				
	CDF-v2	DFDCP	T2I	I2I	FS	FE	
1, 1, 1	90.86	85.01	85.26	84.11	89.91	70.19	84.22
1, 1, 0.25	91.88	86.01	85.26	84.11	89.91	72.19	84.89
1, 2.5, 1	91.82	86.00	85.21	84.08	89.95	71.01	84.67
1, 0.25, 2.5	91.11	85.59	85.09	83.91	89.61	70.92	84.37
1, 2.5, 0.25	94.10	86.66	86.05	84.95	89.42	72.73	<b>85.65</b>

(c) **Experiment on Hyperparameter Configuration.**

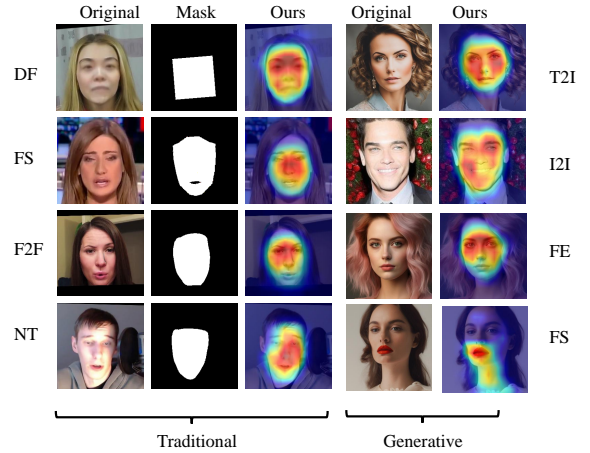


Figure 4. **GradCAM visualization of fake samples across various deepfake datasets.**

an additional 100 epochs to achieve a training loss comparable to that of EfficientNet.

**Impact of hyperparameters.** We also examined the effect of hyperparameters of the loss function on model performance, as detailed in the Table 6c. Our analysis of the weights revealed that increasing the weight of  $\lambda_2$  relative to the weights of cross entropy enhances model performance, whereas decreasing the weight of  $\lambda_3$  relative to cross entropy also improves performance.

## 5. Visualizations

We employed GradCAM [95] to identify the regions activated for forgery detection. The visualization results depicted in Figure 4 demonstrate that our model precisely identifies the areas of deepfake forgery. Beyond visualizing tampered traditional deepfake images, we also conducted visualizations on images produced by state-of-the-art generation techniques.

## 6. Conclusion

In conclusion, this study presents a universal framework for deepfake detection by focusing on common artifacts that span various types of face forgeries. By categorizing deepfake artifacts into Face Inconsistency Artifacts (FIA) and Up-Sampling Artifacts (USA), we enhance the generalization capability of detection models. This targeted approach allows the model to focus on detecting fundamental artifact patterns, and potentially improving its performance across diverse deepfake variations. In doing so, our framework may help address some challenges in current detection methods and could provide a promising foundation for developing more adaptable deepfake detection systems in future research.

## References

- [1] Zhongjie Ba, Qingyu Liu, Zhenguang Liu, Shuang Wu, Feng Lin, Li Lu, and Kui Ren. Exposing the deception: Uncovering more forgery clues for deepfake detection. In *Proceedings of the AAAI Conference on Artificial Intelligence*, pages 719–728, 2024. 6
- [2] Junyi Cao, Chao Ma, Taiping Yao, Shen Chen, Shouhong Ding, and Xiaokang Yang. End-to-end reconstruction-classification learning for face forgery detection. In *Proceedings of the IEEE/CVF Conference on Computer Vision and Pattern Recognition*, pages 4113–4122, 2022. 3, 6, 7
- [3] Liang Chen, Yong Zhang, Yibing Song, Lingqiao Liu, and Jue Wang. Self-supervised learning of adversarial example: Towards good generalizations for deepfake detection. In *Proceedings of the IEEE/CVF conference on computer vision and pattern recognition*, pages 18710–18719, 2022. 2
- [4] Liang Chen, Yong Zhang, Yibing Song, Jue Wang, and Lingqiao Liu. Ost: Improving generalization of deepfake detection via one-shot test-time training. *Advances in Neural Information Processing Systems*, 35:24597–24610, 2022. 2
- [5] Harry Cheng, Yangyang Guo, Tianyi Wang, Liqiang Nie, and Mohan Kankanhalli. Diffusion facial forgery detection. *arXiv preprint arXiv:2401.15859*, 2024. 6
- [6] Jikang Cheng, Zhiyuan Yan, Ying Zhang, Yuhao Luo, Zhongyuan Wang, and Chen Li. Can we leave deepfake data behind in training deepfake detector? *arXiv preprint arXiv:2408.17052*, 2024. 6, 7
- [7] Jongwook Choi, Taehoon Kim, Yonghyun Jeong, Seungryul Baek, and Jongwon Choi. Exploiting style latent flows for generalizing deepfake video detection. In *Proceedings of the IEEE/CVF Conference on Computer Vision and Pattern Recognition (CVPR)*, pages 1133–1143, 2024. 7
- [8] Umur Aybars Ciftci, Ilke Demir, and Lijun Yin. Fakecatcher: Detection of synthetic portrait videos using biological signals. *IEEE transactions on pattern analysis and machine intelligence*, 2020. 3
- [9] Davide Cozzolino, Andreas Rössler, Justus Thies, Matthias Nießner, and Luisa Verdoliva. Id-reveal: Identity-aware deepfake video detection. In *Proceedings of the IEEE/CVF international conference on computer vision*, pages 15108–15117, 2021. 3
- [10] Xinjie Cui, Yuezun Li, Ao Luo, Jiaran Zhou, and Junyu Dong. Forensics adapter: Adapting clip for generalizable face forgery detection. *arXiv preprint arXiv:2411.19715*, 2024. 6
- [11] Hao Dang, Feng Liu, Joel Stehouwer, Xiaoming Liu, and Anil K Jain. On the detection of digital face manipulation. In *Proceedings of the IEEE/CVF Conference on Computer Vision and Pattern recognition*, pages 5781–5790, 2020. 6
- [12] Deepfakedetection, 2021. <https://ai.googleblog.com/2019/09/contributing-data-to-deepfakedetection.html> Accessed 2021-11-13. 6
- [13] DeepFakes, 2020. [www.github.com/deepfakes/faceswap](http://www.github.com/deepfakes/faceswap) Accessed 2020-09-02. 3, 6
- [14] B Dolhansky. The dee pfake detection challenge (dfdc) pre view dataset. *arXiv preprint arXiv:1910.08854*, 2019. 6
- [15] Brian Dolhansky, Joanna Bitton, Ben Pflaum, Jikuo Lu, Russ Howes, Menglin Wang, and Cristian Canton Ferrer. The deepfake detection challenge (dfdc) dataset. *arXiv preprint arXiv:2006.07397*, 2020. 6
- [16] Shichao Dong, Jin Wang, Jiajun Liang, Haoqiang Fan, and Renhe Ji. Explaining deepfake detection by analysing image matching. In *European conference on computer vision*, pages 18–35. Springer, 2022. 3
- [17] Xiaoyi Dong, Jianmin Bao, Dongdong Chen, Ting Zhang, Weiming Zhang, Nenghai Yu, Dong Chen, Fang Wen, and Baining Guo. Protecting celebrities from deepfake with identity consistency transformer. In *Proceedings of the IEEE/CVF Conference on Computer Vision and Pattern Recognition*, pages 9468–9478, 2022. 3, 7
- [18] FaceSwap, 2021. [www.github.com/MarekKowalski/FaceSwap](http://www.github.com/MarekKowalski/FaceSwap) Accessed 2020-09-03. 3, 6
- [19] Jianwei Fei, Yunshu Dai, Peipeng Yu, Tianrun Shen, Zhihua Xia, and Jian Weng. Learning second order local anomaly for general face forgery detection. In *Proceedings of the IEEE/CVF Conference on Computer Vision and Pattern Recognition*, pages 20270–20280, 2022. 3
- [20] Chao Feng, Ziyang Chen, and Andrew Owens. Self-supervised video forensics by audio-visual anomaly detection. In *Proceedings of the IEEE/CVF Conference on Computer Vision and Pattern Recognition*, pages 10491–10503, 2023. 3
- [21] Pierre Foret, Ariel Kleiner, Hossein Mobahi, and Behnam Neyshabur. Sharpness-aware minimization for efficiently improving generalization. *arXiv preprint arXiv:2010.01412*, 2020. 7
- [22] Joel Frank, Thorsten Eisenhofer, Lea Schönherr, Asja Fischer, Dorothea Kolossa, and Thorsten Holz. Leveraging frequency analysis for deep fake image recognition. In *International conference on machine learning*, pages 3247–3258. PMLR, 2020. 2
- [23] Sheldon Fung, Xuequan Lu, Chao Zhang, and Chang-Tsun Li. Deepfakeucl: Deepfake detection via unsupervised contrastive learning. In *2021 international joint conference on neural networks (IJCNN)*, pages 1–8. IEEE, 2021. 3
- [24] Qiqi Gu, Shen Chen, Taiping Yao, Yang Chen, Shouhong Ding, and Ran Yi. Exploiting fine-grained face forgery clues via progressive enhancement learning. In *Proceedings of the*

- AAAI Conference on Artificial Intelligence, pages 735–743, 2022. 3
- [25] Zhihao Gu, Taiping Yao, Yang Chen, Shouhong Ding, and Lizhuang Ma. Hierarchical contrastive inconsistency learning for deepfake video detection. In *European Conference on Computer Vision*, pages 596–613. Springer, 2022. 7
- [26] Hui Guo, Shu Hu, Xin Wang, Ming-Ching Chang, and Siwei Lyu. Eyes tell all: Irregular pupil shapes reveal gan-generated faces. In *ICASSP 2022-2022 IEEE International Conference on Acoustics, Speech and Signal Processing (ICASSP)*, pages 2904–2908. IEEE, 2022. 2
- [27] Xiao Guo, Xiaohong Liu, Zhiyuan Ren, Steven Grosz, Iacopo Masi, and Xiaoming Liu. Hierarchical fine-grained image forgery detection and localization. In *Proceedings of the IEEE/CVF Conference on Computer Vision and Pattern Recognition*, pages 3155–3165, 2023. 3
- [28] Alexandros Haliassos, Konstantinos Vougioukas, Stavros Petridis, and Maja Pantic. Lips don’t lie: A generalisable and robust approach to face forgery detection. In *Proceedings of the IEEE/CVF conference on computer vision and pattern recognition*, pages 5039–5049, 2021. 7
- [29] Alexandros Haliassos, Rodrigo Mira, Stavros Petridis, and Maja Pantic. Leveraging real talking faces via self-supervision for robust forgery detection. In *Proceedings of the IEEE/CVF Conference on Computer Vision and Pattern Recognition*, pages 14950–14962, 2022. 3
- [30] Kaiming He, Xiangyu Zhang, Shaoqing Ren, and Jian Sun. Deep residual learning for image recognition. In *Proceedings of the IEEE conference on computer vision and pattern recognition*, pages 770–778, 2016. 6, 8, 15
- [31] Hillobar, 2023. <https://github.com/Hillobar/Rope>, Accessed 2023. 13, 14
- [32] Edward J Hu, Yelong Shen, Phillip Wallis, Zeyuan Allen-Zhu, Yuanzhi Li, Shean Wang, Lu Wang, and Weizhu Chen. Lora: Low-rank adaptation of large language models. *arXiv preprint arXiv:2106.09685*, 2021. 6
- [33] Shu Hu, Yuezun Li, and Siwei Lyu. Exposing gan-generated faces using inconsistent corneal specular highlights. In *ICASSP 2021-2021 IEEE International Conference on Acoustics, Speech and Signal Processing (ICASSP)*, pages 2500–2504. IEEE, 2021. 2
- [34] Baojin Huang, Zhongyuan Wang, Jifan Yang, Jiabin Ai, Qin Zou, Qian Wang, and Dengpan Ye. Implicit identity driven deepfake face swapping detection. In *Proceedings of the IEEE/CVF conference on computer vision and pattern recognition*, pages 4490–4499, 2023. 7
- [35] Ziqi Huang, Kelvin CK Chan, Yuming Jiang, and Ziwei Liu. Collaborative diffusion for multi-modal face generation and editing. In *Proceedings of the IEEE/CVF Conference on Computer Vision and Pattern Recognition*, pages 6080–6090, 2023. 6
- [36] Yonghyun Jeong, Doyeon Kim, Youngmin Ro, and Jongwon Choi. Freggan: robust deepfake detection using frequency-level perturbations. In *Proceedings of the AAAI conference on artificial intelligence*, pages 1060–1068, 2022. 3
- [37] Tero Karras. Progressive growing of gans for improved quality, stability, and variation. *arXiv preprint arXiv:1710.10196*, 2017. 3
- [38] Tero Karras, Samuli Laine, and Timo Aila. A style-based generator architecture for generative adversarial networks. In *Proceedings of the IEEE/CVF conference on computer vision and pattern recognition*, pages 4401–4410, 2019. 3
- [39] Bahjat Kawar, Shiran Zada, Oran Lang, Omer Tov, Huiwen Chang, Tali Dekel, Inbar Mosseri, and Michal Irani. Imagic: Text-based real image editing with diffusion models. In *Proceedings of the IEEE/CVF Conference on Computer Vision and Pattern Recognition*, pages 6007–6017, 2023. 1, 3, 6
- [40] Kihong Kim, Yunho Kim, Seokju Cho, Junyoung Seo, Jisu Nam, Kychul Lee, Seungrong Kim, and KwangHee Lee. Diffface: Diffusion-based face swapping with facial guidance. *arXiv preprint arXiv:2212.13344*, 2022. 1, 3, 6
- [41] Nicolas Larue, Ngoc-Son Vu, Vitomir Struc, Peter Peer, and Vassilis Christophides. Seeable: Soft discrepancies and bounded contrastive learning for exposing deepfakes. In *Proceedings of the IEEE/CVF International Conference on Computer Vision*, pages 21011–21021, 2023. 2
- [42] Binh M Le and Simon S Woo. Quality-agnostic deepfake detection with intra-model collaborative learning. In *Proceedings of the IEEE/CVF International Conference on Computer Vision*, pages 22378–22389, 2023. 3
- [43] Hanzhe Li, Jiaran Zhou, Bin Li, Junyu Dong, and Yuezun Li. Freqblender: Enhancing deepfake detection by blending frequency knowledge. *arXiv preprint arXiv:2404.13872*, 2024. 2, 7, 13, 14
- [44] Lingzhi Li, Jianmin Bao, Ting Zhang, Hao Yang, Dong Chen, Fang Wen, and Baining Guo. Face x-ray for more general face forgery detection. In *Proceedings of the IEEE/CVF conference on computer vision and pattern recognition*, pages 5001–5010, 2020. 2, 3, 6, 7, 13, 14
- [45] Y Li. Exposing deepfake videos by detecting face warping artifact acts. *arXiv preprint arXiv:1811.00656*, 2018. 6
- [46] Yuezun Li, Ming-Ching Chang, and Siwei Lyu. In ictu oculi: Exposing ai created fake videos by detecting eye blinking. In *2018 IEEE International workshop on information forensics and security (WIFS)*, pages 1–7. Ieee, 2018. 2
- [47] Yuezun Li, Xin Yang, Pu Sun, Honggang Qi, and Siwei Lyu. Celeb-df: A large-scale challenging dataset for deepfake forensics. In *Proceedings of the IEEE/CVF conference on computer vision and pattern recognition*, pages 3207–3216, 2020. 3, 6
- [48] Jiawei Liang, Siyuan Liang, Aishan Liu, Xiaojun Jia, Junhao Kuang, and Xiaochun Cao. Poisoned forgery face: Towards backdoor attacks on face forgery detection. *arXiv preprint arXiv:2402.11473*, 2024. 3
- [49] Tsung-Yi Lin, Piotr Dollár, Ross Girshick, Kaiming He, Bharath Hariharan, and Serge Belongie. Feature pyramid networks for object detection. In *Proceedings of the IEEE conference on computer vision and pattern recognition*, pages 2117–2125, 2017. 4, 15
- [50] Yuzhen Lin, Wentang Song, Bin Li, Yuezun Li, Jiangqun Ni, Han Chen, and Qiushi Li. Fake it till you make it: Curricular dynamic forgery augmentations towards general deepfake detection. In *European Conference on Computer Vision*, pages 104–122. Springer, 2024. 7

- [51] Honggu Liu, Xiaodan Li, Wenbo Zhou, Yuefeng Chen, Yuan He, Hui Xue, Weiming Zhang, and Nenghai Yu. Spatial-phase shallow learning: rethinking face forgery detection in frequency domain. In *Proceedings of the IEEE/CVF conference on computer vision and pattern recognition*, pages 772–781, 2021. 6
- [52] Anwei Luo, Chenqi Kong, Jiwu Huang, Yongjian Hu, Xian-gui Kang, and Alex C. Kot. Beyond the prior forgery knowledge: Mining critical clues for general face forgery detection. *IEEE Transactions on Information Forensics and Security*, 19:1168–1182, 2024. 7
- [53] Yuchen Luo, Yong Zhang, Junchi Yan, and Wei Liu. Generalizing face forgery detection with high-frequency features. In *Proceedings of the IEEE/CVF conference on computer vision and pattern recognition*, pages 16317–16326, 2021. 3, 6
- [54] Midjourney, 2022. <https://www.midjourney.com>, Accessed 2022. 6
- [55] Dat Nguyen, Nesryne Mejri, Inder Pal Singh, Polina Kuleshova, Marcella Astrid, Anis Kacem, Enjie Ghorbel, and Djamilia Aouada. Laa-net: Localized artifact attention network for quality-agnostic and generalizable deepfake detection. In *Proceedings of the IEEE/CVF Conference on Computer Vision and Pattern Recognition*, pages 17395–17405, 2024. 3, 4, 16
- [56] Huy H Nguyen, Junichi Yamagishi, and Isao Echizen. Capsule-forensics: Using capsule networks to detect forged images and videos. In *ICASSP 2019-2019 IEEE international conference on acoustics, speech and signal processing (ICASSP)*, pages 2307–2311. IEEE, 2019. 6
- [57] Yunsheng Ni, Depu Meng, Changqian Yu, Chengbin Quan, Dongchun Ren, and Youjian Zhao. Core: Consistent representation learning for face forgery detection. In *Proceedings of the IEEE/CVF conference on computer vision and pattern recognition*, pages 12–21, 2022. 6, 7
- [58] Trevine Oorloff, Surya Koppiseti, Nicolò Bonettini, Divyraj Solanki, Ben Colman, Yaser Yacoob, Ali Shahriyari, and Gaurav Bharaj. Avff: Audio-visual feature fusion for video deepfake detection. In *Proceedings of the IEEE/CVF Conference on Computer Vision and Pattern Recognition*, pages 27102–27112, 2024. 3
- [59] Dustin Podell, Zion English, Kyle Lacey, Andreas Blattmann, Tim Dockhorn, Jonas Müller, Joe Penna, and Robin Rombach. Sdxl: Improving latent diffusion models for high-resolution image synthesis. *arXiv preprint arXiv:2307.01952*, 2023. 3, 6
- [60] Yuyang Qian, Guojun Yin, Lu Sheng, Zixuan Chen, and Jing Shao. Thinking in frequency: Face forgery detection by mining frequency-aware clues. In *European conference on computer vision*, pages 86–103. Springer, 2020. 3, 6, 7, 17
- [61] Robin Rombach, Andreas Blattmann, Dominik Lorenz, Patrick Esser, and Björn Ommer. High-resolution image synthesis with latent diffusion models. In *Proceedings of the IEEE/CVF conference on computer vision and pattern recognition*, pages 10684–10695, 2022. 2, 3, 4
- [62] Felix Rosberg, Eren Erdal Aksoy, Fernando Alonso-Fernandez, and Cristofer Englund. Facedancer: Pose-and-occlusion-aware high fidelity face swapping. In *Proceedings of the IEEE/CVF winter conference on applications of computer vision*, pages 3454–3463, 2023. 1
- [63] Andreas Rossler, Davide Cozzolino, Luisa Verdoliva, Christian Riess, Justus Thies, and Matthias Nießner. Faceforensics++: Learning to detect manipulated facial images. In *Proceedings of the IEEE/CVF international conference on computer vision*, pages 1–11, 2019. 5, 7
- [64] Nataniel Ruiz, Yuanzhen Li, Varun Jampani, Yael Pritch, Michael Rubinstein, and Kfir Aberman. Dreambooth: Fine tuning text-to-image diffusion models for subject-driven generation. In *CVPR*, pages 22500–22510, 2023. 6
- [65] Somdev Sangwan, 2023. <https://github.com/s0md3v/roop>, Accessed 2023. 13, 14
- [66] Rui Shao, Tianxing Wu, and Ziwei Liu. Detecting and recovering sequential deepfake manipulation. In *European Conference on Computer Vision*, pages 712–728. Springer, 2022. 3, 6
- [67] Kaede Shiohara and Toshihiko Yamasaki. Detecting deepfakes with self-blended images. In *Proceedings of the IEEE/CVF Conference on Computer Vision and Pattern Recognition*, pages 18720–18729, 2022. 2, 3, 6, 7, 13, 14, 17
- [68] Yuyang Sun, Huy H Nguyen, Chun-Shien Lu, ZhiYong Zhang, Lu Sun, and Isao Echizen. Generalized deepfakes detection with reconstructed-blended images and multi-scale feature reconstruction network. *arXiv preprint arXiv:2312.08020*, 2023. 2, 13, 14
- [69] Zhimin Sun, Shen Chen, Taiping Yao, Bangjie Yin, Ran Yi, Shouhong Ding, and Lizhuang Ma. Contrastive pseudo learning for open-world deepfake attribution. In *Proceedings of the IEEE/CVF International Conference on Computer Vision*, pages 20882–20892, 2023. 3
- [70] Chuangchuan Tan, Yao Zhao, Shikui Wei, Guanghua Gu, Ping Liu, and Yunchao Wei. Rethinking the up-sampling operations in cnn-based generative network for generalizable deepfake detection. In *Proceedings of the IEEE/CVF Conference on Computer Vision and Pattern Recognition*, pages 28130–28139, 2024. 2
- [71] Mingxing Tan and Quoc Le. Efficientnet: Rethinking model scaling for convolutional neural networks. In *International conference on machine learning*, pages 6105–6114. PMLR, 2019. 7, 8, 15, 17
- [72] Justus Thies, Michael Zollhofer, Marc Stamminger, Christian Theobalt, and Matthias Nießner. Face2face: Real-time face capture and reenactment of rgb videos. In *Proceedings of the IEEE/CVF Conference on Computer Vision and Pattern Recognition*, 2016. 3, 6
- [73] Justus Thies, Michael Zollhofer, and Matthias Nießner. Deferred neural rendering: Image synthesis using neural textures. *Journal of ACM Transactions on Graphics*, 38(4):1–12, 2019. 3, 6
- [74] Patrick Tinsley, Adam Czajka, and Patrick Flynn. This face does not exist... but it might be yours! identity leakage in generative models. In *Proceedings of the IEEE/CVF Winter Conference on Applications of Computer Vision*, pages 1320–1328, 2021. 3

- [75] Sheng-Yu Wang, Oliver Wang, Richard Zhang, Andrew Owens, and Alexei A Efron. Cnn-generated images are surprisingly easy to spot... for now. In *Proceedings of the IEEE/CVF conference on computer vision and pattern recognition*, pages 8695–8704, 2020. 2, 17
- [76] Xintao Wang, Yu Li, Honglun Zhang, and Ying Shan. Towards real-world blind face restoration with generative facial prior. In *The IEEE Conference on Computer Vision and Pattern Recognition (CVPR)*, 2021. 2, 4
- [77] Xueyu Wang, Jiajun Huang, Siqi Ma, Surya Nepal, and Chang Xu. Deepfake disrupter: The detector of deepfake is my friend. In *Proceedings of the IEEE/CVF Conference on Computer Vision and Pattern Recognition*, pages 14920–14929, 2022. 3
- [78] Zhendong Wang, Jianmin Bao, Wengang Zhou, Weilun Wang, Hezhen Hu, Hong Chen, and Houqiang Li. Dire for diffusion-generated image detection. In *Proceedings of the IEEE/CVF International Conference on Computer Vision*, pages 22445–22455, 2023. 7
- [79] Zhendong Wang, Jianmin Bao, Wengang Zhou, Weilun Wang, and Houqiang Li. Altfreezing for more general video face forgery detection. In *Proceedings of the IEEE/CVF conference on computer vision and pattern recognition*, pages 4129–4138, 2023. 2, 3, 7, 14
- [80] Chen Henry Wu and Fernando De la Torre. A latent space of stochastic diffusion models for zero-shot image editing and guidance. In *Proceedings of the IEEE/CVF International Conference on Computer Vision*, pages 7378–7387, 2023. 1, 3, 6
- [81] Jiahui Wu, Yu Zhu, Xiaoben Jiang, Yatong Liu, and Jiajun Lin. Local attention and long-distance interaction of rppg for deepfake detection. *The Visual Computer*, 40(2):1083–1094, 2024. 3
- [82] Xiaoshi Wu, Keqiang Sun, Feng Zhu, Rui Zhao, and Hongsheng Li. Better aligning text-to-image models with human preference. *arXiv preprint arXiv:2303.14420*, 1(3), 2023. 6
- [83] Yuting Xu, Jian Liang, Gengyun Jia, Ziming Yang, Yanhao Zhang, and Ran He. Tall: Thumbnail layout for deepfake video detection. In *Proceedings of the IEEE/CVF international conference on computer vision*, pages 22658–22668, 2023. 3
- [84] Zhiyuan Yan, Yong Zhang, Yanbo Fan, and Baoyuan Wu. Ucf: Uncovering common features for generalizable deepfake detection. In *Proceedings of the IEEE/CVF International Conference on Computer Vision*, pages 22412–22423, 2023. 2, 6, 7
- [85] Zhiyuan Yan, Yong Zhang, Xinhang Yuan, Siwei Lyu, and Baoyuan Wu. Deepfakebench: A comprehensive benchmark of deepfake detection. *arXiv preprint arXiv:2307.01426*, 2023. 6
- [86] Zhiyuan Yan, Yuhao Luo, Siwei Lyu, Qingshan Liu, and Baoyuan Wu. Transcending forgery specificity with latent space augmentation for generalizable deepfake detection. In *Proceedings of the IEEE/CVF Conference on Computer Vision and Pattern Recognition*, pages 8984–8994, 2024. 2, 3, 6, 7, 13, 14
- [87] Zhiyuan Yan, Taiping Yao, Shen Chen, Yandan Zhao, Xinghe Fu, Junwei Zhu, Donghao Luo, Li Yuan, Chengjie Wang, Shouhong Ding, et al. Df40: Toward next-generation deepfake detection. *arXiv preprint arXiv:2406.13495*, 2024. 3, 6, 7, 16, 17
- [88] Jiwen Yu, Yinhuai Wang, Chen Zhao, Bernard Ghanem, and Jian Zhang. Freedom: Training-free energy-guided conditional diffusion model. In *Proceedings of the IEEE/CVF International Conference on Computer Vision*, pages 23174–23184, 2023. 6
- [89] Ning Yu, Vladislav Skripniuk, Dingfan Chen, Larry Davis, and Mario Fritz. Responsible disclosure of generative models using scalable fingerprinting. *arXiv preprint arXiv:2012.08726*, 2020. 3
- [90] Yike Yuan, Xinghe Fu, Gaoang Wang, Qiming Li, and Xi Li. Forgery-domain-supervised deepfake detection with non-negative constraint. *IEEE Signal Processing Letters*, 29: 2512–2516, 2022. 3
- [91] Cong Zhang, Honggang Qi, Yuezun Li, and Siwei Lyu. Contrastive multi-faceforensics: An end-to-end bi-grained contrastive learning approach for multi-face forgery detection. *arXiv preprint arXiv:2308.01520*, 2023. 3
- [92] Hanqing Zhao, Wenbo Zhou, Dongdong Chen, Tianyi Wei, Weiming Zhang, and Nenghai Yu. Multi-attentional deepfake detection. In *Proceedings of the IEEE/CVF conference on computer vision and pattern recognition*, pages 2185–2194, 2021. 3
- [93] Tianchen Zhao, Xiang Xu, Mingze Xu, Hui Ding, Yuanjun Xiong, and Wei Xia. Learning self-consistency for deepfake detection. In *Proceedings of the IEEE/CVF international conference on computer vision*, pages 15023–15033, 2021. 2, 3, 7
- [94] Yinglin Zheng, Jianmin Bao, Dong Chen, Ming Zeng, and Fang Wen. Exploring temporal coherence for more general video face forgery detection. In *Proceedings of the IEEE/CVF international conference on computer vision*, pages 15044–15054, 2021. 7
- [95] Bolei Zhou, Aditya Khosla, Agata Lapedriza, Aude Oliva, and Antonio Torralba. Learning deep features for discriminative localization. In *Proceedings of the IEEE conference on computer vision and pattern recognition*, pages 2921–2929, 2016. 8
- [96] Wanyi Zhuang, Qi Chu, Zhentao Tan, Qiankun Liu, Haojie Yuan, Changtao Miao, Zixiang Luo, and Nenghai Yu. Uia-vit: Unsupervised inconsistency-aware method based on vision transformer for face forgery detection. In *European conference on computer vision*, pages 391–407. Springer, 2022. 3

## A. Appendix

This supplementary material provides:

- Sec. B: We discussed the classification and basic process of forgery techniques.
- Sec. C: We reviewed the application of data augmentation methods in forgery detection and discussed more details about FIA-USA.
- Sec. D: We introduced the construction process of FPN.
- Sec. E: We provided a detailed introduction to AFFS was provided, along with visual evidence.
- Sec. F: We provide a visualization example of which boundary pixels were discarded by RCR.
- Sec. G: We provided test results on more forgery techniques.
- Sec. H: We provide experimental results combining FIA-USA with other state-of-the-art detection methods.
- Sec. I: We provided more visual examples.

## B. Face forgery techniques

In this section, we discuss the classification of facial forgery technology and the basic process of forgery technology, and at which nodes FIA and USA will be introduced.

### B.1. Classification of facial forgery technology

According to different processing procedures and technical principles, we first divide forgery techniques into two categories:

1). *Full Face Synthesis*: Generate the entire image/video directly through the image / video generation model, without involving facial cropping and stitching in the basic process. Therefore, the artifacts involved in such forgery techniques mainly include USA and a small amount of FIA, where USA is the dependency between adjacent pixels in the forgery area due to the performance of the generator, and FIA is the inconsistency in the generator’s ability to generate face areas with dense details and background areas with sparse details.

2). *Face Swapping*. Crop the original face, generate fake regions through a generator (optional), and then stitch it with the target face. Therefore, this forgery technique can be divided into two situations: a. It includes FIA and USA: FIA is mainly caused by cropping and stitching, as well as generator performance, while USA is mainly determined by generator performance. b. It only includes FIA: FIA is mainly caused by cropping and stitching. Furthermore, based on the forged area, we can divide face swapping into two parts: *Macro-editing* and *Micro-editing*. Macro-editing can be further classified into two subtypes: Editing based on 4 facial keypoints and Editing based on 81 keypoints. Micro-editing allows for precise adjustments to each facial feature.

Figure 5 provides a detailed overview of our classification concept.

### B.2. Basic Process

In Figure 6, we depict the basic process of each type of forgery technique. We can see from this that the main difference between full face synthesis and face swapping lies in whether they include face cropping and stitching operations, which leads to the emergence of a large number of FIA, and whether the background is generated by the generator. The main difference between macro-editing and micro-editing in face swapping is whether the forged

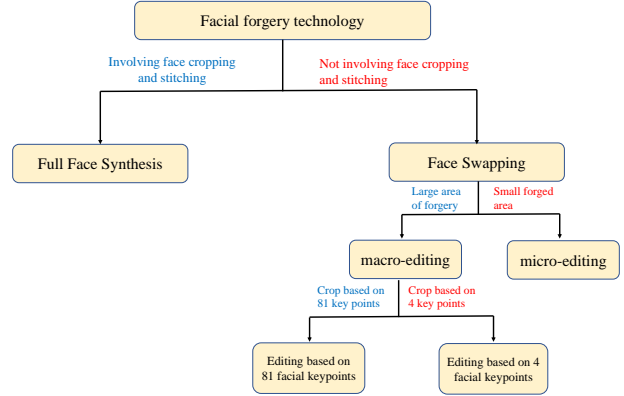


Figure 5. We categorize forgery techniques into two main types: *Full face synthesis* and *Face swapping*. Face swapping is further divided into *macro-editing* (based on 4 or 81 keypoints) and *micro-editing*.

area is the entire face or can finely fabricate facial features. Further, macro editing based on 81 key points is more detailed, and the edges of the forged area are more similar to the edges of a real face, while 4 key points result in the forged area being a square. This discovery is mainly due to a detailed observation of the widely used forgery technique ROPE [31] and roop [65], which provides two types of face cropping techniques.

### B.3. At what stage will FIA and USA be introduced

In Figure 7, we demonstrate which operations lead to the emergence of FIA and USA in the basic process. The observation of a phenomenon led to the refinement of our FIA-USA design.

## C. Details of FIA-USA

### C.1. Blend-based data augmentation

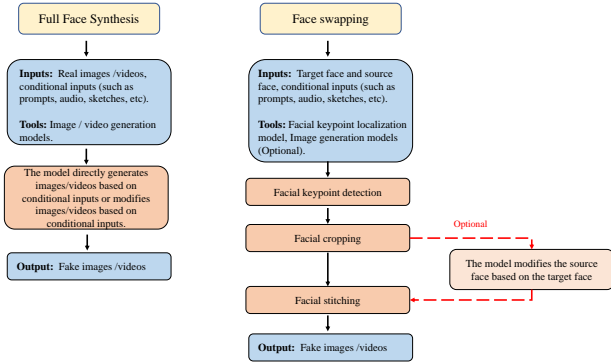
In Deepfake detection, a successful approach is to manually construct negative samples for training, where data augmentation in the RGB domain is based on Blend, which can be represented as follows:

$$I_F = M \odot I_t + (1 - M) \odot I_s, \quad (7)$$

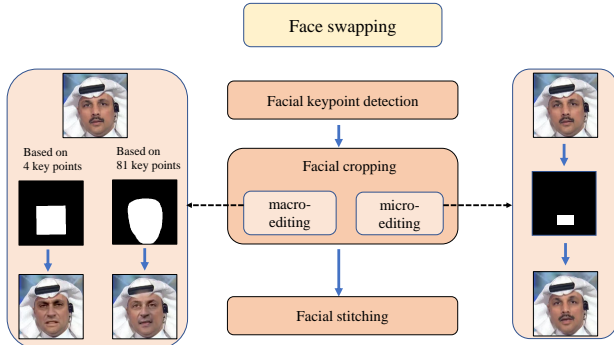
Among them,  $I_t$  represents the target face,  $I_s$  represents the source face, and  $I_F$  represents the negative sample. The earliest design [44] was to use facial similarity to find the most suitable  $I_s$  for  $I_t$ . Later, SBI [67] proposed self-blend to improve the statistical consistency of  $I_F$ . There are also works [68] that separate the background and face of  $I_t$ , add noise to the background, and reconstruct  $I_t$ , using the reconstructed  $I_t$  for blend. However, to our knowledge, there has been no work so far that considers the introduction of both global and local artifacts, let alone the introduction of FIA at both the full face and regional levels while introducing USA.

### C.2. Other types of data augmentation

In recent years, many other data augmentation methods have been proposed, such as frequency domain [43] and latent space [86].



(a) Basic processes of *full face synthesis* and *face swapping*.



(b) Basic processes of *macro-editing* (4 vs 81 keypoints) and *micro-editing*

Figure 6. We illustrate the basic processes of forgery techniques, *full face synthesis* and *face swapping* differ in face cropping and stitching, while *macro-editing* (4 vs 81 keypoints) and *micro-editing* vary in forgery scope and detail.

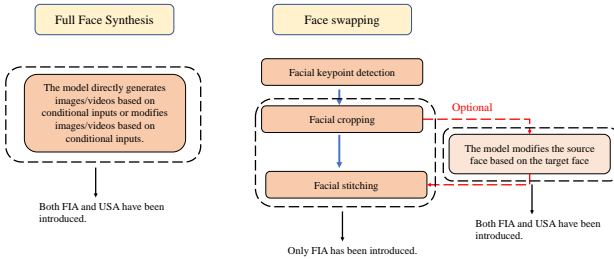


Figure 7. The operations that led to the occurrence of FIA and USA in the basic process.

Many studies suggest [43, 86] that compared to data augmentation in other domains, data augmentation in the RGB domain [44, 67, 68] exhibits weak robustness and limited effectiveness. However, we have demonstrated through extensive experiments that our proposed data augmentation in the RGB domain is not weaker or even better than that in other domains. It is worth mentioning that our proposed data augmentation belongs to the image level, and we surprisingly found that it is superior to the most advanced data augmentation methods at the video level [79].

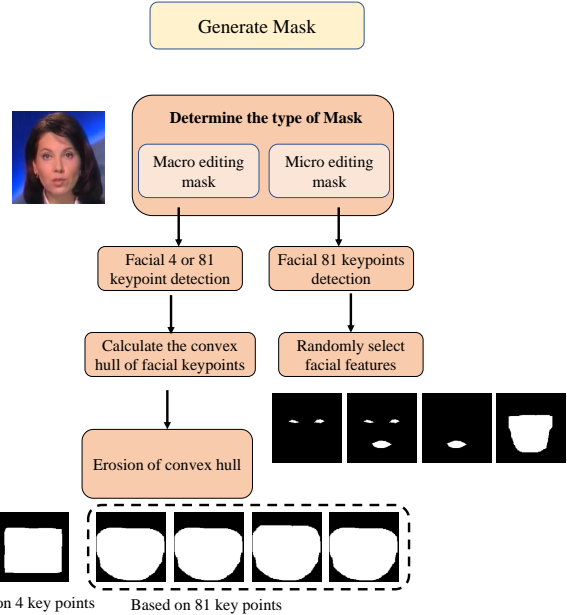


Figure 8. The generation of macro and micro-editing masks in FIA-USA, using convex hull and erosion / expansion for macro masks and random feature combination for micro masks.

### C.3. The detailed process of generating masks in FIA-USA

Here we have detailed the processing of generating masks in FIA-USA, as shown in Figure 8. Firstly, we divide mask generation into two types: 1) Macro editing masks and 2) Micro editing masks.

**Macro editing mask:** We follow the mask generation process in SBI [67], which includes the following steps: a. Calculate the convex hull of 81 facial keypoints to obtain the mask of facial contour b. Erosion or expansion of the mask; Besides, we also considered the case of calculating convex hull based on 4 facial keypoints, which originated from the observation of two methods for extracting raw faces provided by the open-source deepfake project that is truly available [31, 65].

**Micro-editing masks:** The main method is to simulate the forgery process of manipulating facial details randomly by randomly combining facial features.

### C.4. Why use Autoencoder and Super-Resolution models to reconstruct images

As shown in Figure 9, we divide the processing flow of the generative model into two categories: One category generates images of forged regions that are clear and free of blur as the original image (using Diffusion models and GANs as the main methods, and upsampling the latent code through AE to generate images). And another type (especially older voice driven lip shape modification techniques) will result in blurred tampered areas, requiring additional facial super-resolution models to process the blurred areas. Therefore, we use autoencoder (AE) to reconstruct images or facial Super-Resolution (SR) to process faces, in order to approximate the USA introduced by the generator in the forged area.

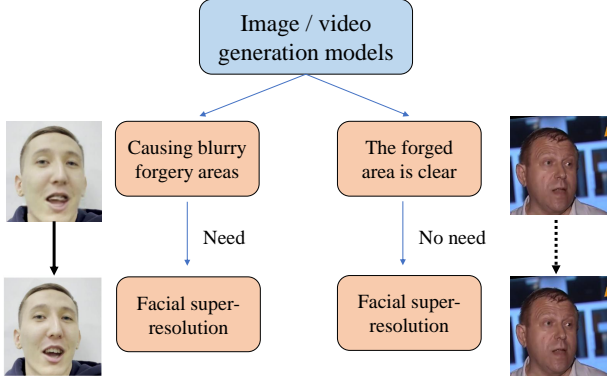


Figure 9. We divide the generation models into two categories based on whether facial super-resolution models is needed for post-processing.

### C.5. FIA-USA covers all possible situations that may occur in FIA and USA

As shown in the Figure 10, our proposed FIA-USA framework covers every possible situation that may occur in FIA and USA, which is also the most intuitive explanation why our method is effective.

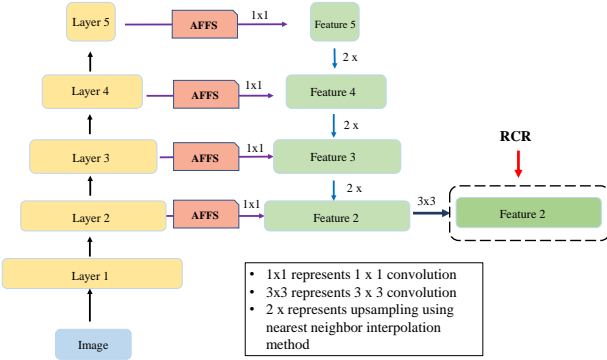


Figure 11. We illustrated the construction process of FPN.

## D. Details of FPN

As shown in the Figure 11, our FPN follows the framework proposed by Lin et al., using the output features of the 2nd, 3rd, 4th, and 5th layers of the backbone to construct an FPN. In our experimental setup, the number of feature map channels is 128 and 196, corresponding to EfficientNet [71], and Resnet [30], respectively.

## E. Details of AFFS

Here we provide a detailed description of the process of AFFS and a visual explanation of its effectiveness.

### E.1. Why is AFFS proposed

Let’s consider a neural network  $\phi$  and an FPN  $P$ , as well as the process of performing RCR on the FPN’s maximum resolution

layer. The output of  $\phi$  is a set of features  $\{d_1, d_2, d_3, d_4\}$ ,  $P$  takes this set of features as input to construct a set of feature maps with same dimensions and different resolutions, while RCR performs feature differentiation learning on the feature map with the highest resolution. One intuition is that there is a significant amount of redundancy in the output features of the  $\phi$ , and not every dimension of the features  $d_i, i \in [1, 2, 3, 4]$  is suitable for constructing FPN for RCR. Therefore, we propose AFFS for feature dimensionality reduction of each feature  $d_i$  before constructing FPN. Moreover, this feature dimensionality reduction method effectively exploits the potential advantages of our proposed FIA-USA and lays the foundation for the effective execution of RCR.

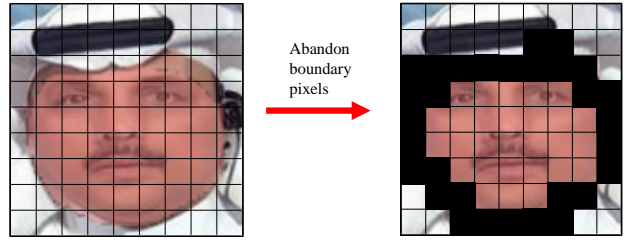


Figure 12. We provide a visual example to illustrate which pixels will be discarded.

### E.2. AFFS

Here, we will provide a more comprehensive explanation of the workflow of AFFS from a different perspective.

1) First, let’s consider multiple positive and negative sample pairs generated by FIA-USA, along with their corresponding masks  $\{R_n, F_n, M_n\}_{n=1}^N$ . The usual method is to directly construct an FPN using a set of features  $f_i$  from a neural network  $\phi$  as input, where  $i$  represents the  $i$ -th layer of the  $\phi$ . We can see that this process is not related to FIA-USA, so it cannot fully unleash the potential of FIA-USA, and the constructed feature pyramid also intuitively lays the foundation for RCR.

2) Next, let’s discuss the initialization process of AFFS. For the output of each layer of the neural network, we hope that the difference between the real image and the fake image after normalization is as consistent as possible with the mask  $M$  used to represent forged areas. However, we have noticed that not every channel meets this requirement, so we would like to reserve channels that meet the requirements for each layer. Therefore, for  $f_i \in \mathbb{R}^{W_i * H_i * C_i}$ , we calculate the following loss for each channel on a set of FIA-USA generated samples  $\{R_n, F_n, M_n\}_{n=1}^N$  to obtain those excellent dimensions,

$$\mathcal{L}_{AFFS}^{i,k} = \frac{1}{N} \sum_{n=1}^N \|\mathcal{F}(f_i^k(R_n) - (f_i^k(F_n)) - M_n)\|_2^2 \quad (8)$$

$\mathcal{F}$  represents normalization and scaling operations,  $f_i^k \in \mathbb{R}^{W_i * H_i}$ ,  $k \in [0, C_i]$ , represents the feature map of the  $k$ -th dimension of the  $f_i$ . During the training process, we only select the channels reserved for  $f_i$  during the AFFS initialization process. After AFFS processing, the original features  $f_i \in \mathbb{R}^{W_i * H_i * C_i}$  will become  $f_i' \in \mathbb{R}^{W_i * H_i * m_i}$

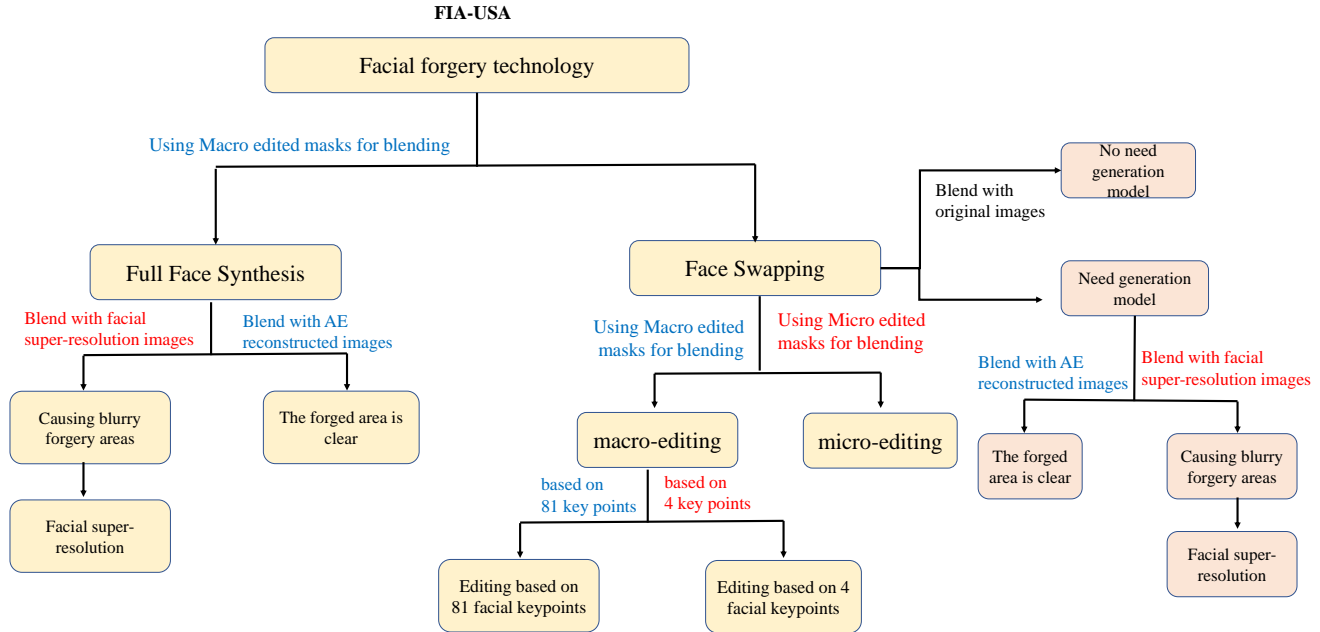


Figure 10. We demonstrate through graphical representation that our proposed FIA-USA covers all possible scenarios that may lead to the occurrence of FIA and USA.

### E.3. Visual Explanation of AFFS

Here we provide a set of visual examples of AFFS in Figure 13. The experiment was conducted on the 2-th layer of Efficient-NetB4. Unlike the actual situation, in order to enhance readability, we only calculated  $L_{AFFS}$  for a single epoch on a single pair of samples. And based on this, sort the 32 dimensions of the features in the 2-th layer. Here, we present the dimensions ranked in the top 14 and bottom 4. In the actual process, we iterate for 5 epochs on all samples on the training set to initialize AFFS. In Table 7, we present the changes in feature dimensions of different backbone features before and after performing AFFS

Model	Input Dimension	Output Dimension
Res50	{256,512,1024,2048}	{196,384,768,1536}
Res101	{256,512,1024,2048}	{196,384,768,1536}
Effb1	{24,40,112,320}	{16,24,40,112}
Effb4	{32,56,160,448}	{24,32,56,160}

Table 7. Feature dimension parameters of AFFS.

Method	Training set	CDF	DFDCP	Avg.
LAA-Net	FF++(C23) +SBI	0.840	0.741	0.791
LAA-Net	FF++(C23) +FIA-USA	0.875	0.782	0.829

Table 8. We report the Video-level AUC. The combination of our data augmentation method with other Sota detection algorithms.

### F. Details of RCR

In the LAA Net [55], a very interesting hypothesis is the pixels on the fake boundary contain both the features of the fake area and the features of the real area, so in our designed RCR, such pixels will be discarded. Figure 12 provides a visual example.

### G. Testing on more forgery techniques

In addition to several widely used forgery detection datasets mentioned in the paper, we also conducted experiments on other sota forgery techniques based on the DF40 dataset [87], where real samples were obtained from FF++ and fake samples were constructed using corresponding forgery techniques based on FF++ settings. As shown in the Table 9a, our proposed forgery detection framework has achieved excellent detection results on the vast majority of forgery methods. Meanwhile, Table 9b shows the comparison between our method and other state-of-the-art methods on various forgery techniques in DIFF

### H. Combining with SoTA detection method

In this section, we plan to combine our proposed FIA-USA data augmentation with other sota image-level detection methods to validate the effectiveness of our proposed data augmentation method. However, due to the limited availability of open-source image level detection methods, we can only provide the performance of our data augmentation method on LAA-Net [55] (CVPR 24) in Table 8. In the original paper, the model was trained on the FF++ dataset in the raw version, while here we trained on the C23 version.

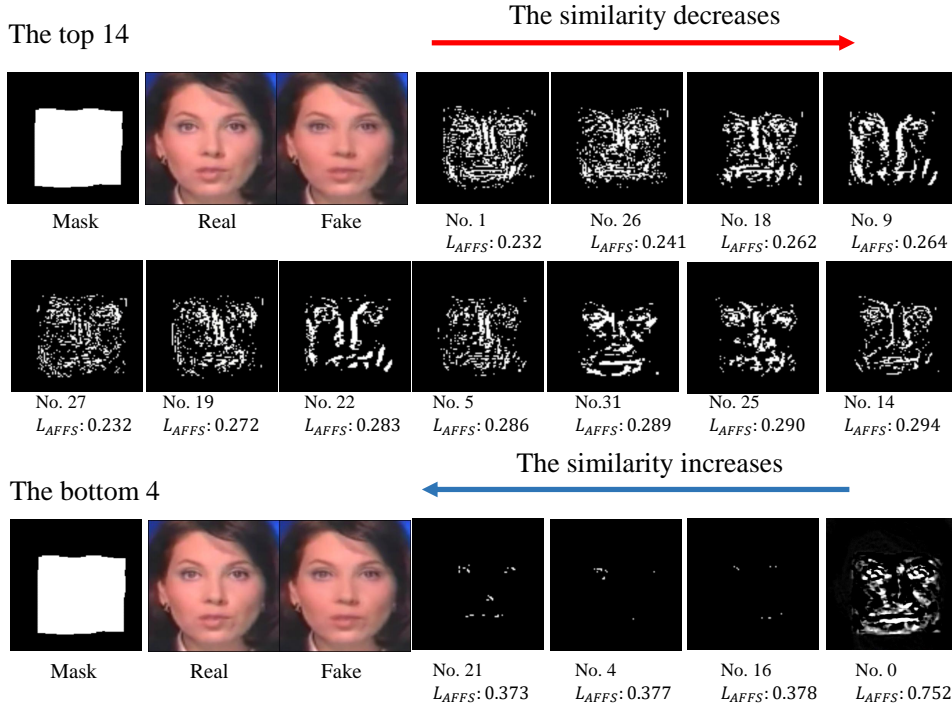


Figure 13. The result of calculating  $L_{AFFS}$  for the 32 dimensions of the 2-th layer features of EfficientNetB4 on a single sample and sorting them by similarity.

Type	mobileswap	MidJourney	faceswap	styleclip	DiT	lia	ddim	mcnet	RDDM	StyleGAN3
AUC	0.97	0.97	0.89	0.82	0.66	0.91	0.97	0.84	0.70	0.93
Type	e4e	pixart	whichfaceisreal	deepfaceclab	StyleGANXL	heygen	facedancer	MRAA	pirender	VQGAN
AUC	0.95	0.93	0.42	0.77	0.41	0.58	0.83	0.85	0.81	0.85
Type	StyleGAN2	facevid2vid	simsmap	inswap	one_shot_free	wav2lip	e4s	starganv2	tpsm	sd2.1
AUC	0.93	0.83	0.91	0.87	0.85	0.76	0.88	0.48	0.83	0.97
Type	blendface	hyperreenact	uniface	CollabDiff	fsgan	danet	SiT	sadtalker	fomm	
AUC	0.94	0.80	0.92	0.95	0.86	0.80	0.72	0.74	0.85	

(a) We tested all forgery techniques provided on the DF40 dataset and reported Frame-Level AUC.

Method	Train Set		Test Subset												
	Real	Fake	Cycle	CoDiff	Imagic	DiFace	DCFace	Dream	SDXL_R	FD.I	LoRA	Midj	FD.T	SDXL	HPS
F <sup>3</sup> -Net <sup>†</sup> [60]	✓	✓	36.14	35.00	32.56	25.61	53.29	55.45	65.04	40.90	-	-	45.00	61.64	68.96
EfficientNet <sup>†</sup> [71]	✓	✓	56.51	38.38	48.50	64.45	89.13	71.64	65.04	59.93	-	-	69.67	64.94	74.63
CNN_Aug <sup>‡</sup> [75]	✓	✓	50.31	46.84	75.95	43.10	80.69	58.75	60.10	43.65	-	-	47.90	61.95	60.56
SBI <sup>†</sup> [67]	✓		82.32	64.70	49.84	73.64	89.92	75.66	77.73	87.67	89.18	79.56	90.55	80.37	83.30
Ours	✓		84.76	72.61	52.92	76.86	93.63	83.43	80.54	92.68	93.48	82.57	94.85	82.15	88.40

(b) Comparison with universal deepfake detection methods using the Frame-Level AUC on the DiFF dataset. The notation <sup>†</sup> indicates models that are designed for deepfake detection, while <sup>‡</sup> signifies models intended for general generated detection. All experiments were trained on the c23 version of FF++.

Table 9. Test results on more forgery techniques.

## I. More visual examples

From Figure 14 to Figure 16, we demonstrate the fake samples that FIA-USA can generate through different reconstruction methods, including autoencoderr (AE) and facial super-resolution (SR), and

multiple types of masks based on three real faces. Figure 17 shows the negative samples randomly generated by FIA-USA during the real training process. Figures 18 to 22 list the images in the DF40 dataset [87] that were misclassified by our method.

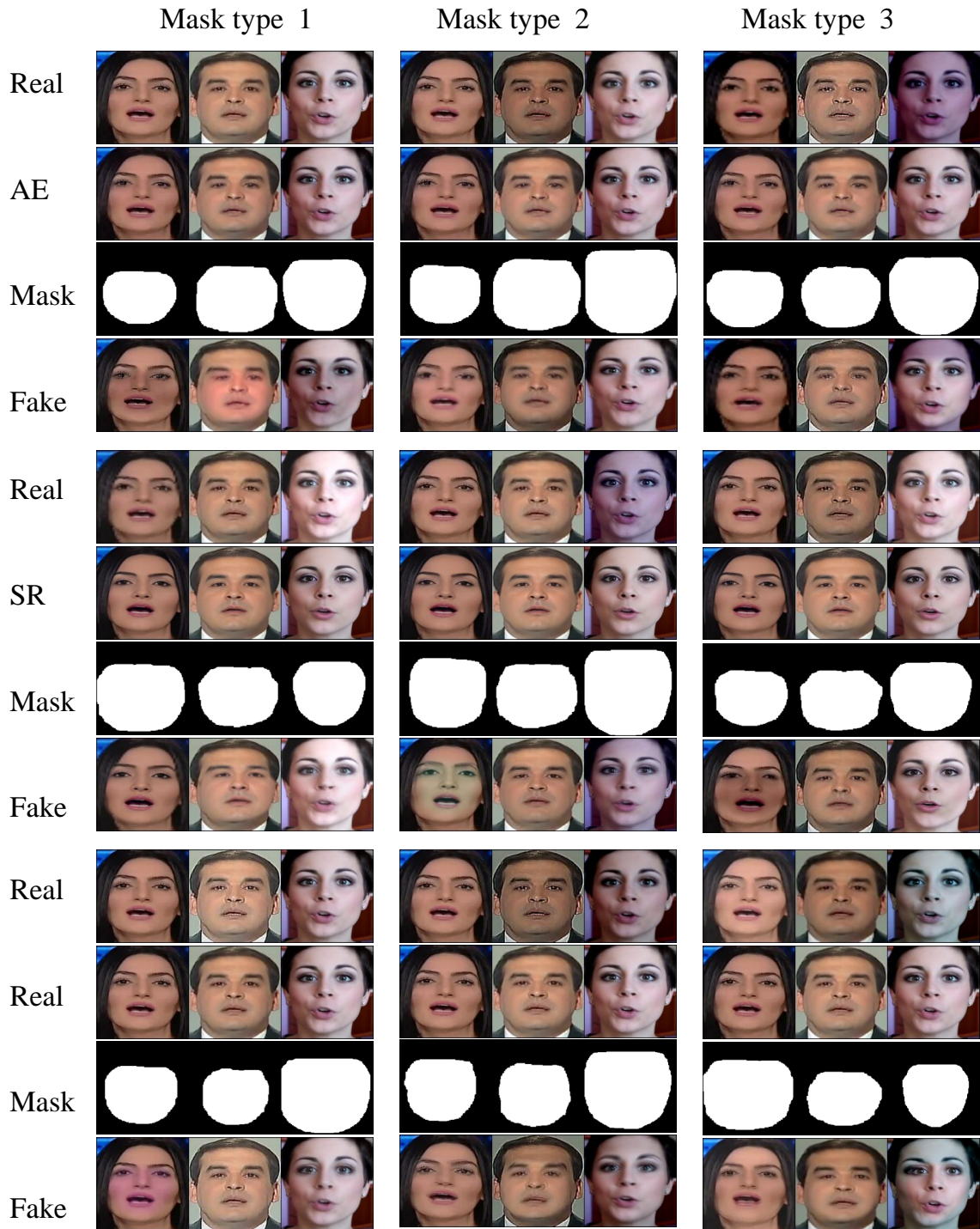


Figure 14. More examples of FIA-USA.

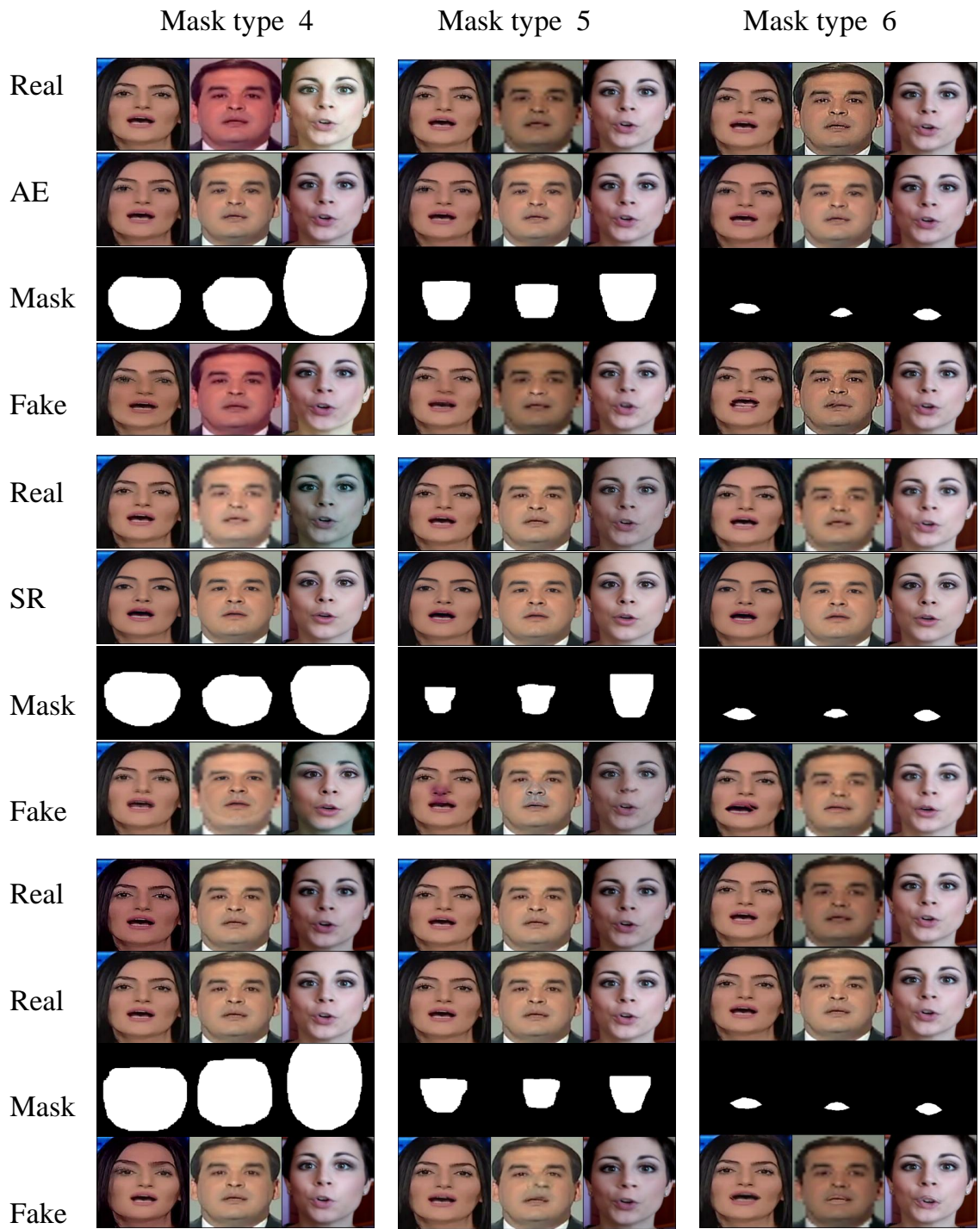


Figure 15. More examples of FIA-USA.

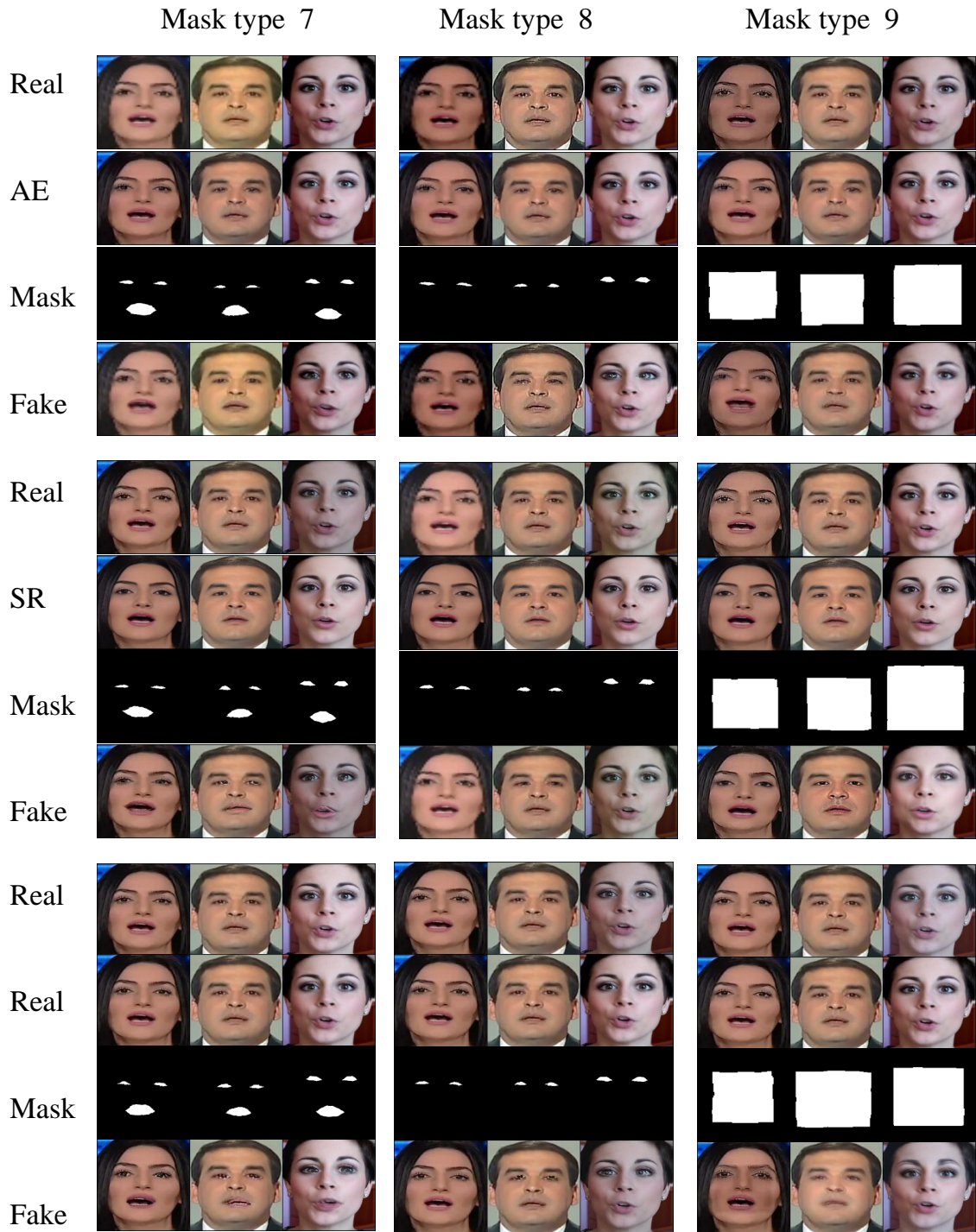


Figure 16. More examples of FIA-USA.

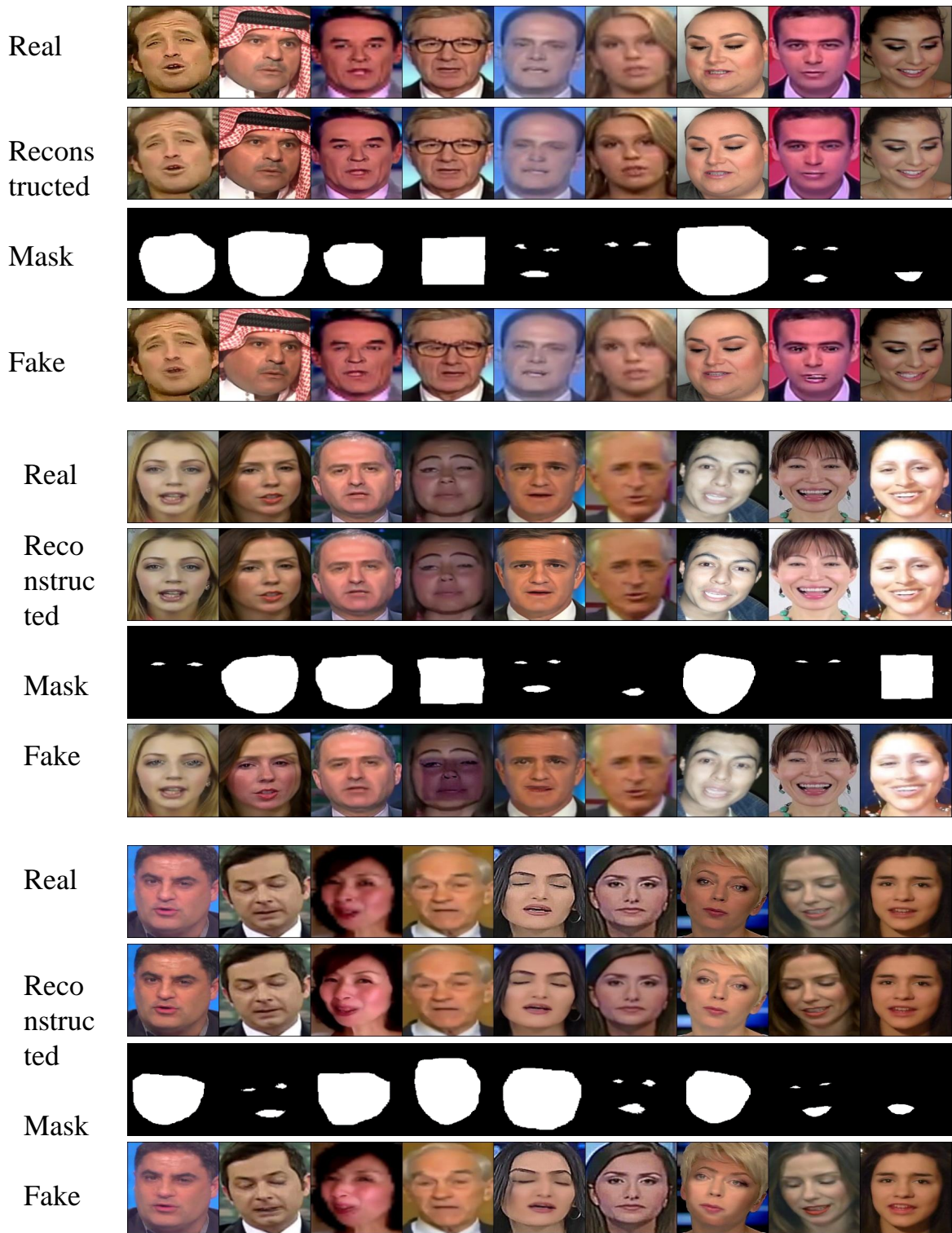


Figure 17. More examples of FIA-USA.

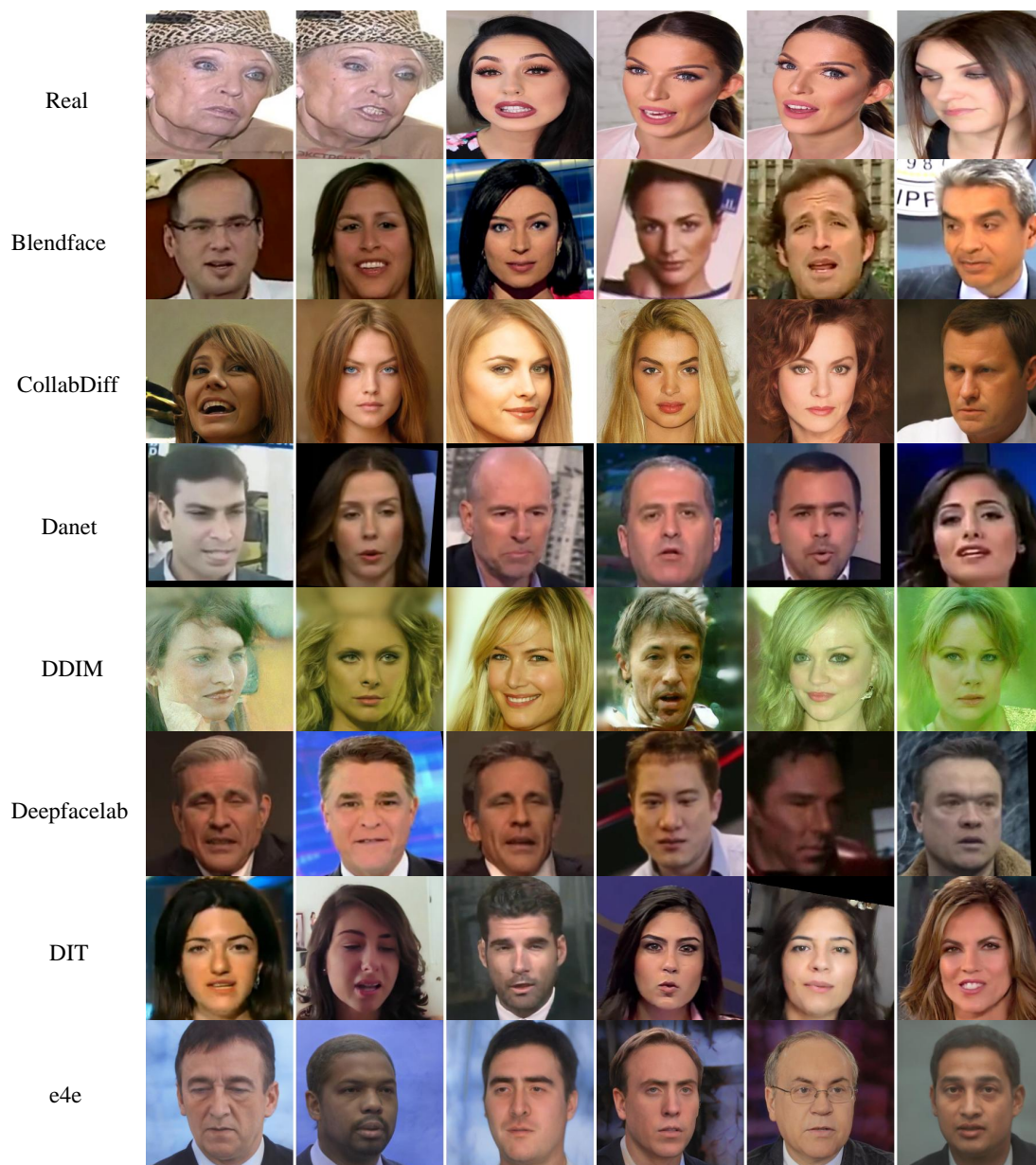


Figure 18. Images misclassified by our method in the DF40 dataset.

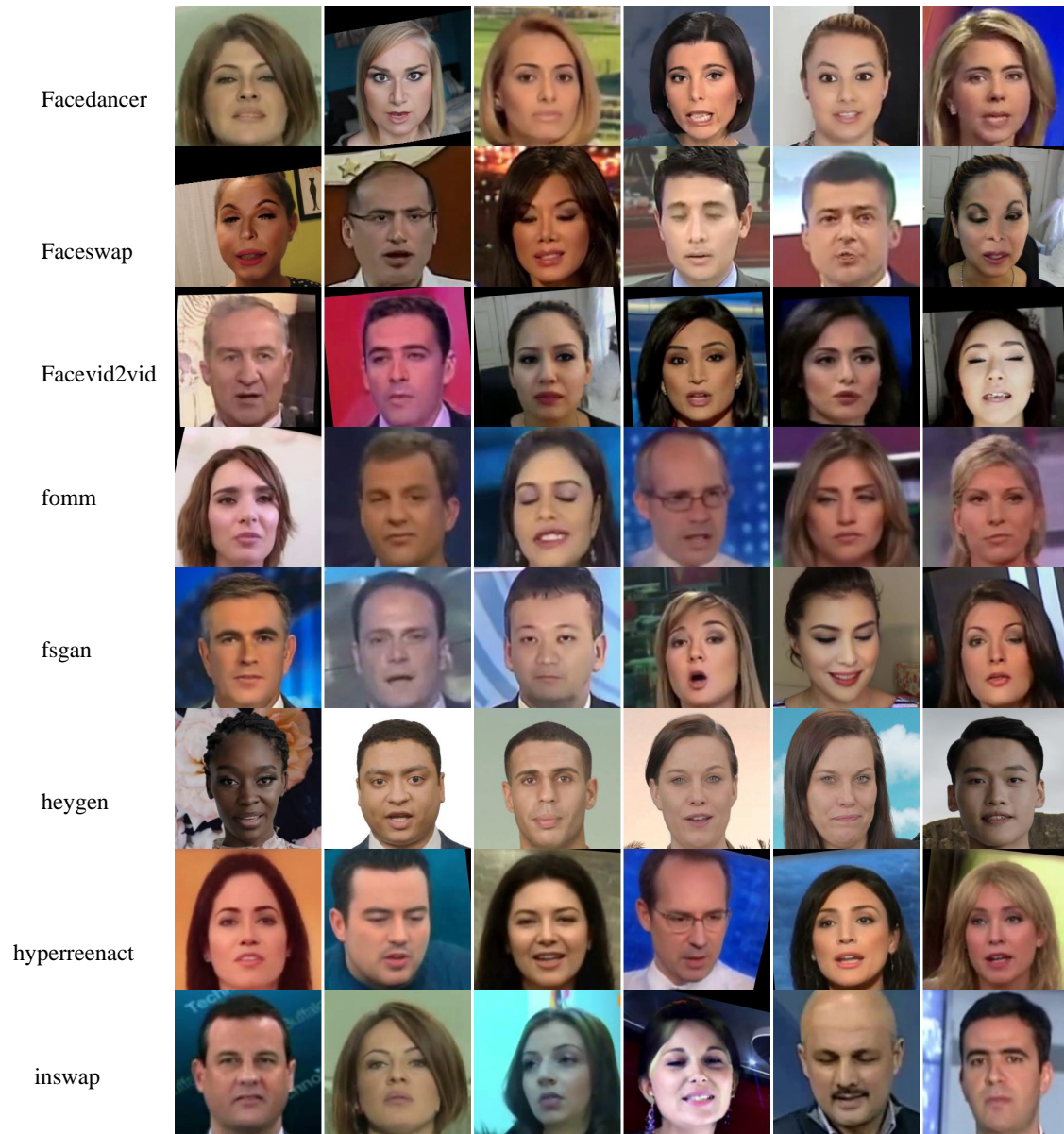


Figure 19. Images misclassified by our method in the DF40 dataset.

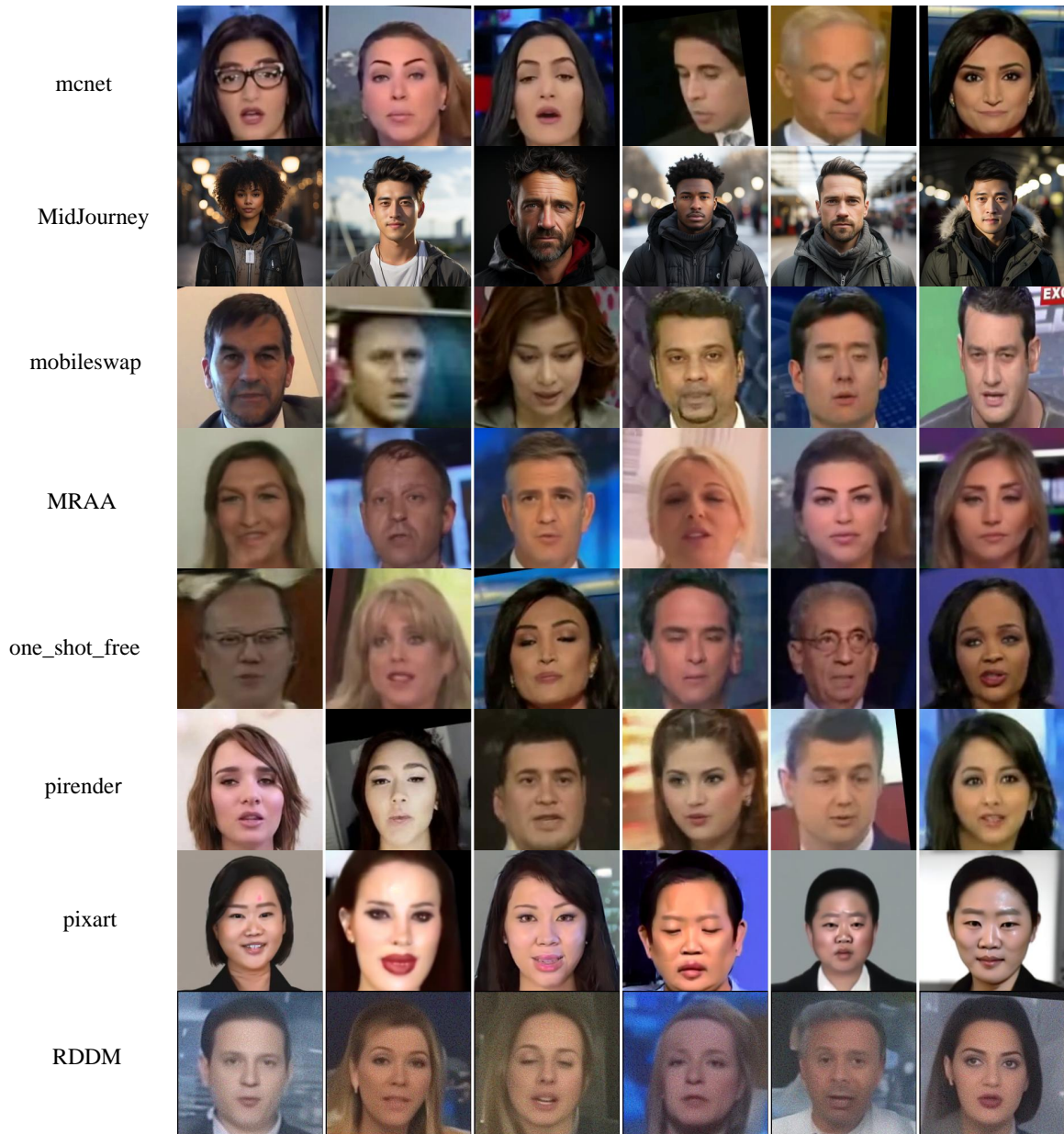


Figure 20. Images misclassified by our method in the DF40 dataset.

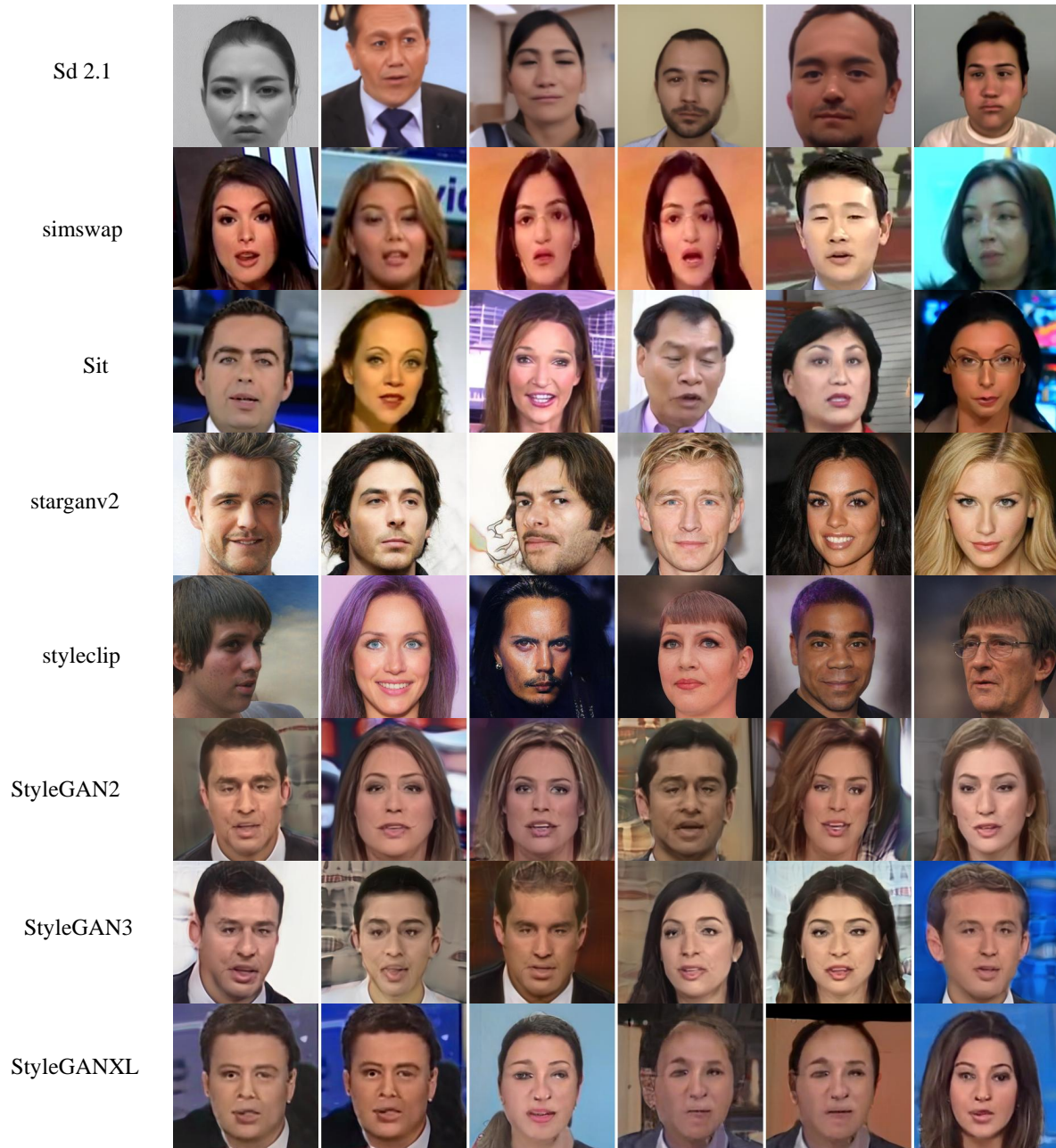


Figure 21. Images misclassified by our method in the DF40 dataset.

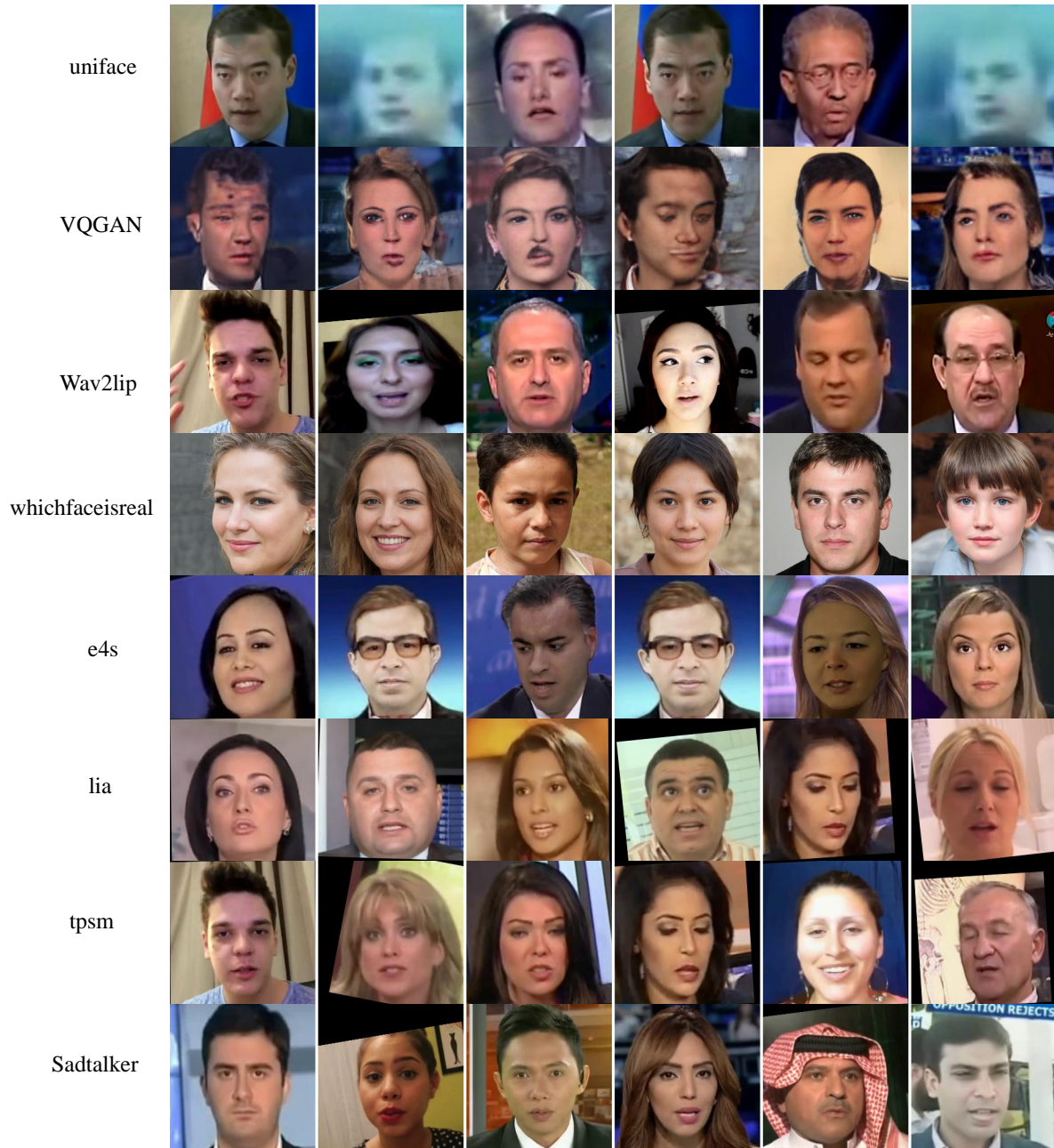


Figure 22. Images misclassified by our method in the DF40 dataset.